

University of Windsor Scholarship at UWindsor

Electronic Theses and Dissertations

1996

Retro-reflective optics to determine stress resulting from interlaminar corrosion in fuselage lap joints.

Qin, Geng
University of Windsor

Follow this and additional works at: <http://scholar.uwindsor.ca/etd>

Recommended Citation

Geng, Qin., "Retro-reflective optics to determine stress resulting from interlaminar corrosion in fuselage lap joints." (1996). *Electronic Theses and Dissertations*. Paper 3347.

This online database contains the full-text of PhD dissertations and Masters' theses of University of Windsor students from 1954 forward. These documents are made available for personal study and research purposes only, in accordance with the Canadian Copyright Act and the Creative Commons license—CC BY-NC-ND (Attribution, Non-Commercial, No Derivative Works). Under this license, works must always be attributed to the copyright holder (original author), cannot be used for any commercial purposes, and may not be altered. Any other use would require the permission of the copyright holder. Students may inquire about withdrawing their dissertation and/or thesis from this database. For additional inquiries, please contact the repository administrator via email (scholarship@uwindsor.ca) or by telephone at 519-253-3000ext. 3208.



National Library
of Canada

Acquisitions and
Bibliographic Services Branch

395 Wellington Street
Ottawa, Ontario
K1A 0N4

Bibliothèque nationale
du Canada

Direction des acquisitions et
des services bibliographiques

395, rue Wellington
Ottawa (Ontario)
K1A 0N4

Your file / Votre référence

Our file / Notre référence

NOTICE

The quality of this microform is heavily dependent upon the quality of the original thesis submitted for microfilming. Every effort has been made to ensure the highest quality of reproduction possible.

If pages are missing, contact the university which granted the degree.

Some pages may have indistinct print especially if the original pages were typed with a poor typewriter ribbon or if the university sent us an inferior photocopy.

Reproduction in full or in part of this microform is governed by the Canadian Copyright Act, R.S.C. 1970, c. C-30, and subsequent amendments.

AVIS

La qualité de cette microforme dépend grandement de la qualité de la thèse soumise au microfilmage. Nous avons tout fait pour assurer une qualité supérieure de reproduction.

S'il manque des pages, veuillez communiquer avec l'université qui a conféré le grade.

La qualité d'impression de certaines pages peut laisser à désirer, surtout si les pages originales ont été dactylographiées à l'aide d'un ruban usé ou si l'université nous a fait parvenir une photocopie de qualité inférieure.

La reproduction, même partielle, de cette microforme est soumise à la Loi canadienne sur le droit d'auteur, SRC 1970, c. C-30, et ses amendements subséquents.

**Retro-reflective Optics to Determine Stress
Resulting from Interlaminar Corrosion
in Fuselage Lap Joints**

by

Qin Geng

A Thesis Submitted to the
Faculty of Graduate Studies and Research through
the Department of Mechanical and Materials Engineering
in Partial Fulfillment of the Requirements for
the Degree of Master of Applied Science
at the University of Windsor

Windsor, Ontario, Canada
1996



National Library
of Canada

Acquisitions and
Bibliographic Services Branch

395 Wellington Street
Ottawa, Ontario
K1A 0N4

Bibliothèque nationale
du Canada

Direction des acquisitions et
des services bibliographiques

395, rue Wellington
Ottawa (Ontario)
K1A 0N4

Your file *Votre référence*

Our file *Notre référence*

The author has granted an irrevocable non-exclusive licence allowing the National Library of Canada to reproduce, loan, distribute or sell copies of his/her thesis by any means and in any form or format, making this thesis available to interested persons.

L'auteur a accordé une licence irrévocable et non exclusive permettant à la Bibliothèque nationale du Canada de reproduire, prêter, distribuer ou vendre des copies de sa thèse de quelque manière et sous quelque forme que ce soit pour mettre des exemplaires de cette thèse à la disposition des personnes intéressées.

The author retains ownership of the copyright in his/her thesis. Neither the thesis nor substantial extracts from it may be printed or otherwise reproduced without his/her permission.

L'auteur conserve la propriété du droit d'auteur qui protège sa thèse. Ni la thèse ni des extraits substantiels de celle-ci ne doivent être imprimés ou autrement reproduits sans son autorisation.

ISBN 0-612-10995-X

Canada

Name QIN GENG

Dissertation Abstracts International and Masters Abstracts International are arranged by broad, general subject categories. Please select the one subject which most nearly describes the content of your dissertation or thesis. Enter the corresponding four-digit code in the spaces provided.

Mechanical Engineering

SUBJECT TERM

0548

UMI

SUBJECT CODE

Subject Categories

THE HUMANITIES AND SOCIAL SCIENCES

COMMUNICATIONS AND THE ARTS	
Architecture	0729
Art History	0377
Cinema	0900
Dance	0378
Fine Arts	0357
Information Science	0723
Journalism	0391
Library Science	0399
Mass Communications	0708
Music	0413
Speech Communication	0459
Theater	0465
EDUCATION	
General	0515
Administration	0514
Adult and Continuing	0516
Agricultural	0517
Art	0273
Bilingual and Multicultural	0282
Business	0688
Community College	0275
Curriculum and Instruction	0727
Early Childhood	0518
Elementary	0524
Finance	0277
Guidance and Counseling	0519
Health	0650
Higher	0745
History of	0320
Home Economics	0278
Industrial	0521
Language and Literature	0279
Mathematics	0280
Music	0522
Philosophy of	0998
Physical	0523

Psychology	0525
Reading	0535
Religious	0527
Sciences	0714
Secondary	0533
Social Sciences	0534
Sociology of	0340
Special	0529
Teacher Training	0530
Technology	0710
Tests and Measurements	0288
Vocational	0747

LANGUAGE, LITERATURE AND LINGUISTICS

Language	
General	0679
Ancient	0289
Linguistics	0290
Modern	0291
Literature	
General	0401
Classical	0294
Comparative	0295
Medieval	0297
Modern	0298
African	0316
American	0591
Asian	0305
Canadian (English)	0352
Canadian (French)	0355
English	0593
Germanic	0311
Latin American	0312
Middle Eastern	0315
Romance	0313
Slavic and East European	0314

PHILOSOPHY, RELIGION AND THEOLOGY

Philosophy	0422
Religion	
General	0318
Biblical Studies	0321
Clergy	0319
History of	0320
Philosophy of	0322
Theology	0469
SOCIAL SCIENCES	
American Studies	0323
Anthropology	
Archaeology	0324
Cultural	0326
Physical	0327
Business Administration	
General	0310
Accounting	0272
Banking	0770
Management	0454
Marketing	0338
Canadian Studies	0385
Economics	
General	0501
Agricultural	0503
Commerce-Business	0505
Finance	0508
History	0509
Labor	0510
Theory	0511
Folklore	0358
Geography	0366
Gerontology	0351
History	
General	0578

Ancient	0579
Medieval	0581
Modern	0582
Black	0320
African	0331
Asia, Australia and Oceania	0332
Canadian	0334
European	0335
Latin American	0336
Middle Eastern	0333
United States	0337
History of Science	0585
Law	0398
Political Science	
General	0615
International Law and Relations	
Public Administration	0617
Recreation	0814
Social Work	0452
Sociology	
General	0626
Criminology and Penology	0627
Demography	0938
Ethnic and Racial Studies	0631
Individual and Family Studies	
Industrial and Labor Relations	0629
Public and Social Welfare	0630
Social Structure and Development	
Theory and Methods	0700
Transportation	0709
Urban and Regional Planning	0999
Women's Studies	0453

THE SCIENCES AND ENGINEERING

BIOLOGICAL SCIENCES

Agriculture	
General	0473
Agronomy	0285
Animal Culture and Nutrition	
Animal Pathology	0476
Food Science and Technology	
Forestry and Wildlife	0478
Plant Culture	0479
Plant Pathology	0480
Plant Physiology	0817
Range Management	0777
Wood Technology	0746
Biology	
General	0306
Anatomy	0287
Biostatistics	0308
Botany	0309
Cell	0379
Ecology	0329
Entomology	0353
Genetics	0349
Limnology	0793
Microbiology	0410
Molecular	0307
Neuroscience	0317
Oceanography	0416
Physiology	0433
Radiation	0821
Veterinary Science	0778
Zoology	0472
Biophysics	
General	0786
Medical	0760
EARTH SCIENCES	
Biogeochemistry	0425
Geochemistry	0996

Geodesy	0370
Geology	0372
Geophysics	0373
Hydrology	0388
Mineralogy	0411
Paleobotany	0345
Paleoecology	0426
Paleontology	0418
Paleozoology	0985
Palynology	0427
Physical Geography	0368
Physical Oceanography	0415

HEALTH AND ENVIRONMENTAL SCIENCES

Environmental Sciences	
General	0768
Health Sciences	
General	0566
Audiology	0300
Chemotherapy	0992
Dentistry	0567
Education	0350
Hospital Management	0769
Human Development	0758
Immunology	0982
Medicine and Surgery	0564
Mental Health	0347
Nursing	0569
Nutrition	0570
Obstetrics and Gynecology	0380
Occupational Health and Therapy	
Ophthalmology	0381
Pathology	0571
Pharmacology	0419
Pharmacy	0572
Physical Therapy	0382
Public Health	0573
Radiology	0574
Recreation	0575

Speech Pathology	0460
Toxicology	0383
Home Economics	0386

PHYSICAL SCIENCES

Pure Sciences	
Chemistry	
General	0485
Agricultural	0749
Analytical	0486
Biochemistry	0487
Inorganic	0488
Nuclear	0738
Organic	0490
Pharmaceutical	0491
Physical	0494
Polymer	0495
Radiation	0754
Mathematics	0405
Physics	
General	0605
Acoustics	0986
Astronomy and Astrophysics	
Atmospheric Science	0606
Atomic	0608
Electronics and Electricity	0748
Elementary Particles and High Energy	0607
Fluid and Plasma	0798
Molecular	0759
Nuclear	0609
Optics	0610
Radiation	0752
Solid State	0756
Statistics	0611
Applied Sciences	0463
Applied Mechanics	0346
Computer Science	0984

Engineering	
General	0537
Aerospace	0538
Agricultural	0539
Automotive	0540
Biomedical	0541
Chemical	0542
Civil	0543
Electronics and Electrical	0544
Heat and Thermodynamics	0348
Hydraulic	0545
Industrial	0546
Marine	0547
Materials Science	0794
Mechanical	0548
Metallurgy	0743
Mining	0551
Nuclear	0552
Packaging	0549
Petroleum	0765
Sanitary and Municipal	0554
System Science	0790
Geotechnology	0428
Operations Research	0796
Plastics Technology	0795
Textile Technology	0994

PSYCHOLOGY

General	0621
Behavioral	0384
Clinical	0622
Developmental	0620
Experimental	0623
Industrial	0624
Personality	0625
Physiological	0989
Psychobiology	0349
Psychometrics	0632
Social	0451

AD C478E

© 1996, Qin Geng

ABSTRACT

A systematic inspection process was developed to locate and measure the sub surface damage of aging aircraft. This process included four steps. First, D Sight technology was used to identify and locate pillowing deformations in an aircraft fuselage. Second, Ultrasonic Inspection was used to detect the degree of corrosion in a small localized deformation area. And then, LVDT Contour Measurement was conducted to determine the amplitude of pillowing deformation. Finally, Finite Element techniques in conjunction with the mathematical method were used to evaluate the magnitude of the flexure stress superposed on the deformed skin.

D Sight has been proven as an effective method for large surface inspection. Ultrasonic Detection showed the applicability of interlaminar corrosion identification. LVDT Contour Measurement facilitates quantitative interpretation of the effect of corrosion build-up. The FEA model was developed and was proved to be useful tool for the measurement of stress. This combination process provides a new approach in the evaluation of an aging aircraft fuselage.

Dedicated to
my parents and my brother

ACKNOWLEDGEMENTS

This thesis would not have been possible without the guidance, patience, and support of Dr. W. P. North and the late Dr. V. M. Huynh.

Many thanks and gratitude are owed to my colleagues, faculty, and staff members of the Mechanical and Materials Engineering department at the University of Windsor whose friendship, encouragement, and assistance I greatly appreciated while pursuing my education.

Finally, I heartily thank my parents and my brother for their sacrifice of my being away from them and for their love and understanding during my study.

TABLE OF CONTENTS

ABSTRACT	iv
DEDICATION	v
ACKNOWLEDGEMENTS	vi
TABLE OF CONTENTS	vii
LIST OF FIGURES	ix
LIST OF TABLES	xi
NOMENCLATURE	xii
CHAPTER 1. INTRODUCTION AND OBJECTIVES	1
CHAPTER 2. LITERATURE REVIEW	3
CHAPTER 3. EXPERIMENTAL WORK	6
3.1 D Sight	6
3.1.1 Introduction to D Sight	6
3.1.2 Purpose	8
3.1.3 Method	9
3.1.4 Observation and Results	9
3.1.4.1 Effect of On Axis vs. Off Axis	12
3.1.4.2 Effect of Light Source Aperture	12
3.2 Contour Measurements	17
3.2.1 Purpose	17
3.2.2 Method	17
3.2.3 Results	18
3.3 Ultrasonic Inspection	24
3.3.1 Introduction to Ultrasonic Inspection	24
3.3.2 Method	24
3.3.3 Results	29

CHAPTER 4. MATHEMATICAL MODEL	35
4.1 Purpose	35
4.2 Method	35
4.3 Results	38
CHAPTER 5. FINITE ELEMENT STRESS ANALYSIS	45
5.1 Purpose	45
5.2. Method	45
5.2.1 Whole Plate Model	45
5.2.2 Quarter Plate Model	47
5.3. Results	50
5.3.1 Mesh Density	50
5.3.2 Stress Analysis	50
CHAPTER 6. CONCLUSIONS	55
CHAPTER 7. RECOMMENDATIONS	57
REFERENCES	59
VITA AUCTORIS	63

LIST OF FIGURES

FIGURES:

Figure 1	Basic D Sight arrangement	7
Figure 2	Photograph of actual D Sight setup	10
Figure 3	The D Sight image of the lap joints	11
Figure 4	1 mm aperture light source - on axis	13
Figure 5	1 mm aperture light source - off axis	14
Figure 6	5 mm aperture light source - off axis	15
Figure 7	25 mm aperture light source - off axis	16
Figure 8	Schematic of LVDT setup	19
Figure 9	Photograph of LVDT setup	20
Figure 10	Close-up of the LVDTs	21
Figure 11	Computer results of contour measurement	22
Figure 12	3-D plot of the LVDT data	23
Figure 13	Schematic of ultrasonic transducer	26
Figure 14	Photograph of ultrasonic setup	27
Figure 15	Close-up photograph of the ultrasonic test	28
Figure 16	Ultrasonic B-scan	30
Figure 17	C-scan showing interlaminar corrosion at a rivet	31

Figure 18	Photograph of rivet with severe corrosion	32
Figure 19	Photograph of rivet with light corrosion	33
Figure 20	Photograph of rivet without corrosion	34
Figure 21	Mathematical model - plate	37
Figure 22	Mathematical model - segment	43
Figure 23	Schematic of an actual lap joint	46
Figure 24	FEA boundary conditions - quarter plate	48
Figure 25	FEA displacement of - quarter plate	53
Figure 26	FEA stress distribution - quarter plate	54

LIST OF TABLES

Table 1	Material properties used in FEA models	47
Table 2	Maximum displacement for various mesh densities	49
Table 3	Theoretical and FEA results	51
Table 4	Von Mises stress profile through the plate thickness	51

NOMENCLATURE

x,y,z	Rectangular coordinates
a,b	Distance between rivets
h	Thickness of a plate
q	Applied pressure
w	Plate deflection
E	Modulus of elasticity in tension and compression
ν	Poisson's ratio
D	Flexural rigidity of a plate
Q_x, Q_y	Shearing forces parallel to z axis per unit length of sections of a plate perpendicular to x and y axes, respectively
M_x, M_y	Bending moments per unit length of sections of a plate perpendicular to x and y axes, respectively
σ_x, σ_y	Normal components of stress parallel to x and y

CHAPTER 1

INTRODUCTION AND OBJECTIVES

More than 3,000 of the world's 9,000 commercial aircraft are past their life expectancy of 20 years and current economics suggests that they have to be used for much longer. With the continual operation of these airplanes, there is a concern that significant corrosion combined with fatigue damage could lead to a catastrophic failure. Since the total elimination of airplane structure corrosion is impossible, it becomes necessary to be able to detect corrosion at a level that has little effect on airplane integrity.

The stressed skin of the fuselage is formed from thin aluminum sheet(skin) which is joined by riveting the connections. Since these connections cannot be sealed from the atmosphere, interlayer corrosion of this type of connection occurs over long periods of exposure and in the presence of cyclic stress, fatigue cracks initiate and propagate.

The contact pressure between the aluminum skin and structure as a result of the riveting is insufficient to prevent moisture from entering this interface. This corrosion and fretting action results in a small amount of pillowing distortion between the rivets of the connection. The magnitude of the pillowing is an indication of the sub surface damage in the connection and is used in the inspection process to identify where damage is likely to be located. This oxidation and resulting pillowing of the aluminum also induces flexure

stress which is superposed on the operational stresses. This in turn results in fatigue cracks at the stress concentration caused by the rivets.

In this research, an investigation of the inspection process in an attempt to quantify the sub surface damage will be developed in a four stage objective.

1. To use D Sight to rapidly identify very small localized deformations in the skin of an external aircraft fuselage.
2. To evaluate the amplitude of the deformation of the outer skin and to generate a simulated actual shape of the pillowing.
3. To determine if ultrasonic technology can be used to identify interlaminar corrosion and to measure the thickness loss in the skin.
4. To evaluate the magnitude of the flexure stress superposed on the design as a result of this corrosion driven phenomenon.

A sample of a fuselage lap joint which was retrieved from a retired aircraft in the Mojave Desert in California (one of the largest aircraft storage locations) was used in all the experiments of this research.

CHAPTER 2

LITERATURE REVIEW

Corrosion detection in transport aircraft is a difficult problem since a significant amount of corrosion occurs in hidden areas. Corrosion behind aluminum skin panels and on contacting surfaces has historically been detected either by "pillowing", which occurs due to the growth of corrosion products behind the surface, or when through-the-thickness corrosion is present.

The primary method, specified by the aircraft industry for detecting corrosion, is visual inspection, which is not entirely reliable and which may leave corrosion undetected until an advanced stage.

The main nondestructive inspection (NDI) techniques employed for monitoring the growth of corrosion are x-ray radiography, eddy current, shadow moire, thermal wave imagery, ultrasonic, etc.

A report from AGARD¹ (Advisory Group for Aerospace Research & Development) shows that the x-ray results were largely disappointing, in that they failed to detect any corrosion in most of these specimens even those that revealed significant amounts of corrosion on tear down and during visual inspection.

It also shows that the eddy current testing was less effective on some Douglas

specimens than on the Boeing specimens because of the higher aspect ratio of the fastener arrangements in the former. The Boeing lap joints normally have rivet spacings of about an inch, in the longitudinal as well as circumferential direction. The inter-rivet spacing on the Douglas specimens is about an inch and a half in the circumferential direction and only a third of that in the longitudinal direction. This close spacing caused spurious results in the eddy current tests since a probe with a diameter of 3/8" had to be used for scanning the specimens. Similarly the proximity of the rivet row to the edge of the outer skin of the Douglas joints also resulted in loss of sensitivity of the eddy current probe in this region.

These traditional techniques do not appear to have the sensitivity that's needed and can be time consuming and expensive.

Clark, Reynolds, and Pryor² have patented the technique used for visually exaggerating surface distortions, depressions or protrusions which has been adapted as a rapid, enhanced visual inspection method for inspection of large external aircraft surfaces. This technology is marketed by Diffracto Ltd. under the trademark D-Sight. Attempts by Diffracto to quantify the grey level image in order to produce general contour information have had limited success.

Komorowski, Gould, and Pastorius³ used D Sight to detect impact damage to composite aircraft structure and Komorowski, Simpson, and Gould⁴ describe its use on metal aircraft to detect cold-worked holes, cracks, and surface corrosion.

The report from Structures, Materials and Propulsion Laboratory at Institute for

Aerospace Research⁵ shows that aluminum oxide trihydrate is the main corrosion product in lap joints. The volume of this oxide is more than six times greater than the aluminum from which it originated. And the pillowing deformation due to this large volumetric increase is greater than the corrosion thickness loss.

Bellinger, Krishnakumar and Komorowski⁶ developed a model to predict the extent of the corrosion within a joint in terms of thickness loss at the internal surfaces from the amplitude of the pillowing of the outer skin.

Recently developed nondestructive inspection (NDI) methods have been able to detect reductions in skin thickness greater than 10% of nominal thickness⁷. However, such procedures are still of limited value since most of the aircraft structure is limited to a thickness loss of 10% before it is replaced due to corrosion damage.

CHAPTER 3

EXPERIMENTAL WORK

3.1. D Sight

3.1.1. Introduction to D Sight

D SIGHT is an optical process that converts local surface curvature changes into greyscale changes. This enhanced surface inspection technique is used for visualizing surface distortions, depressions or protrusions. The process has excellent sensitivity (down to 2 micron surface height change) and a large dynamic range. The sensitivity is adjustable by changing the system optical parameters, a feature that allows tailoring to specific applications.

Figure 1 shows the basic elements required for the D SIGHT process: A camera unit consisting of a CCD camera and a point light source, the surface being inspected and a retro reflective screen(retroreflector). The light from the point light source spreads and strikes the surface where it is reflected onto the retro reflective screen. The retro-reflector (in this case 3M Scotchlite) is made up of very small (25-75 μ m dia), high refractive index glass beads with a silvered reflective coating on the back, bonded to a flexible sheet. This screen returns the light to the surface where it is reflected back to the light source. If any irregularities exist in the surface, the uniform light field upon striking the surface of the

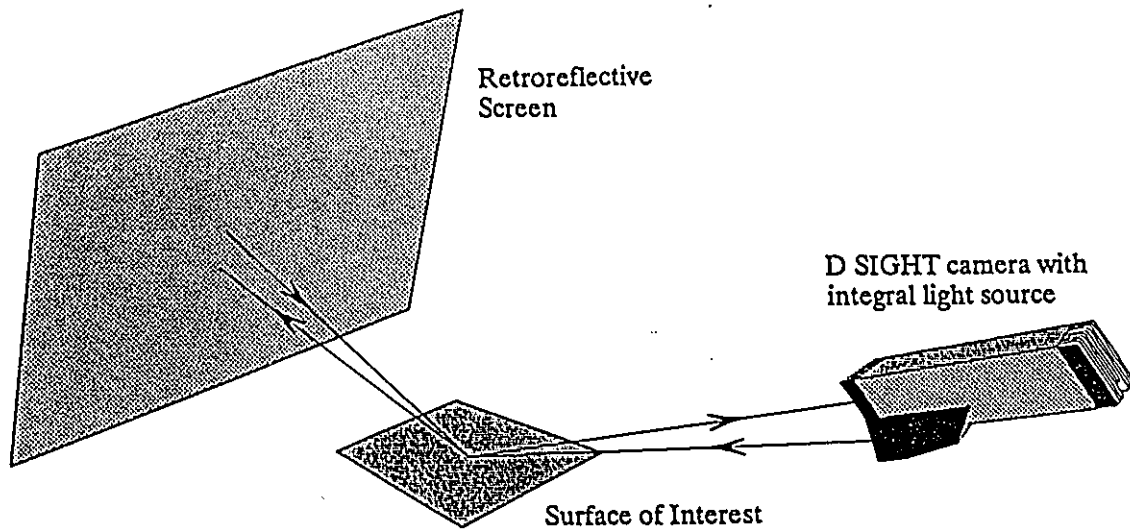


Figure 1. Basic D Sight arrangement

specimen will become distorted, and the light field will now have varying grey levels upon striking the retro reflective screen. If the screen were a perfect retro-reflector, each ray of light would follow the exact same path along the optical axis back to the light source. Furthermore, upon being re-reflected back from the specimen surface, all the distortions occurring to the light field from the first reflection will simply be reversed, i.e., a uniform light field will return to the source. However, the retro reflective screen is not perfect, such as the glass bead type, (the light is slightly scattered) and returns a cone of light to the light source via the surface. The rays in the diverging cone of light will not trace their incident path back to the light source. When this different path is followed, then the rays in the diverging cone of light will not reflect from the specimen at the exact same point they did the first pass, thus not reversing the distortions in the light intensity field that occurred from the first reflection. Since the rays in this diverging cone do not return precisely to the light source, they may be detected by an outside source, such as a camera, or human eye. Provided that the camera is very close to the optical axis of the incident light source, the intensity variation of the light seen by the camera is therefore a map of the surface curvature variations on the surface being inspected. This local surface curvature map is referred to as the D SIGHT image and can be directly used to indicate surface quality or can be used to infer subsurface conditions.

3.1.2. Purpose

The purpose was to use the D Sight optical procedure to rapidly identify very small

localized deformations in large aircraft panels.

3.1.3. Method

In this experiment the sample was viewed using D Sight. The photographic setup is shown in Figure 2. The distance from the camera to the sample was 1.5 m and from the sample to the retro-reflector was 1 m. The light from the fiber optic point light source was bounced off the surface of the sample to a retroflective screen. The image on this screen was viewed through the reflection on the surface of the sample from a location slightly (25-50 mm) off axis to the fiber optic light source.

The image of the object of interest was captured by the camera, and a separate monitor was used to display images. The video output from the CCD camera was digitized by a high performance 6-bit PCEyes digitizer board and a PC-386 computer. The digitizer board in conjunction with the VGA board can produce a binary picture with a resolution of 640 x 480 pixels with with 64 levels of grey scale. The images were photographed or video-recorded for documentation purposes.

3.1.4. Observations and Results

Figure 3 shows the D Sight image of the sample. It indicates that the pillowing only occurs at one end of the sample. It can be seen that the very small localized deformation is visually exaggerated and can be easily identified.

Camera and point light source

Retro-reflector

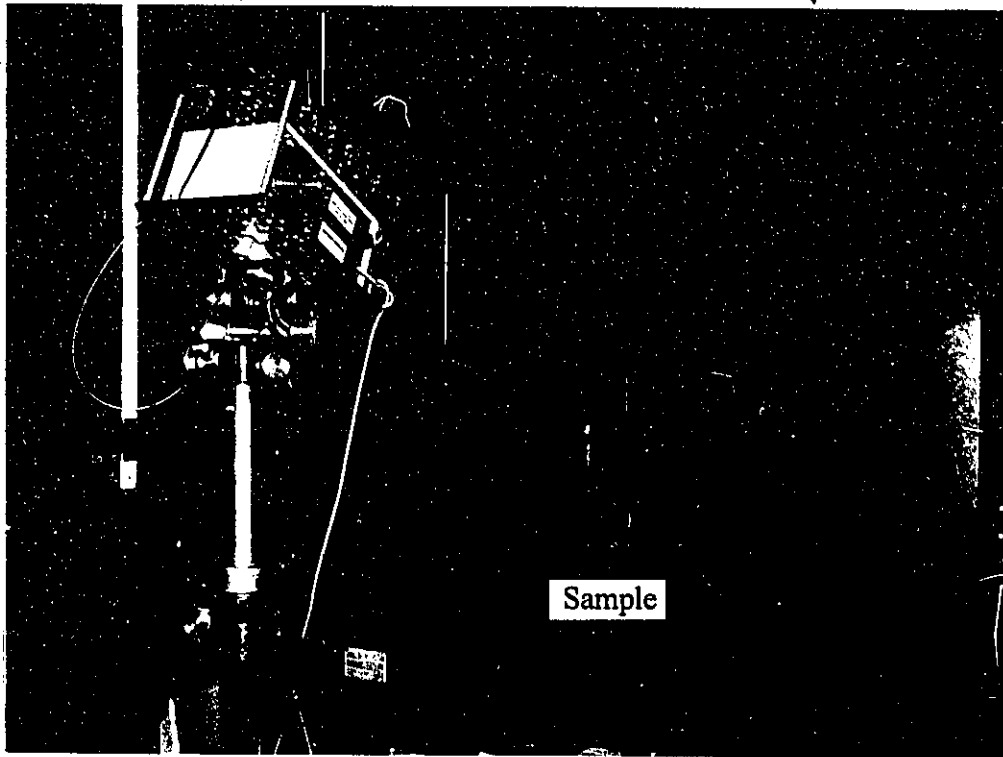


Figure 2. Photograph of actual D Sight setup

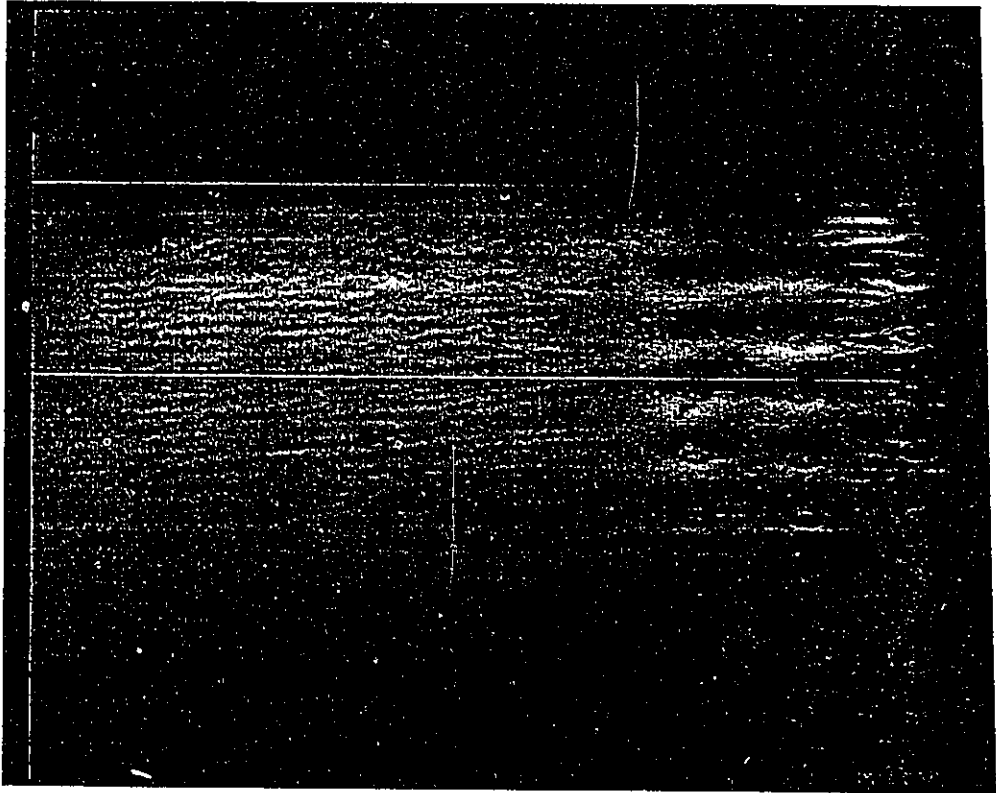


Figure 3. The D Sight image of the lap joints

Experiments were conducted using the fiber optic at different positions. For example: on axis, off axis, as well as a differing size of point light source, in this case, a very small aperture (1 mm), a larger aperture (5 mm), and a diffuse light source (25 mm).

3.1.4.1. Effect of on axis vs. off axis

When a perfectly flat surface was observed in this setup, uniform light intensity was observed over the surface. The lap joint was observed when the 1 mm aperture light source was put on axis and off axis. The results were shown in Figure 4 and 5, respectively. The intensity in Figure 5 depends on the offset of the imaging lens - the smaller the offset, the higher the intensity. The change of intensity is fairly rapid with the change in the offset distance as the retro-reflector is quite efficient. The on-axis arrangement is clearly superior.

3.1.4.2. The effect of light source aperture

An offset light source of 5 mm aperture and 25 mm aperture were used in Figure 6 and 7. The sensitivity of retro reflection for contour visualization is inversely proportional to the size of the illumination source. In order to obtain the highest resolution possible using retroreflection, the smallest aperture light source is obviously preferred.

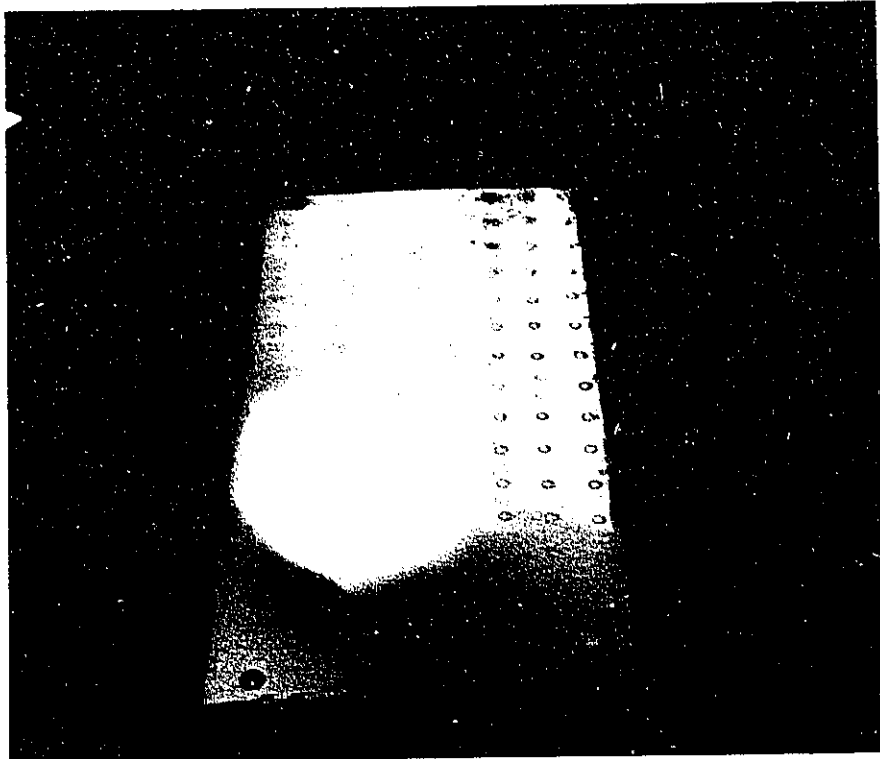


Figure 4. 1 mm aperture light source - on axis

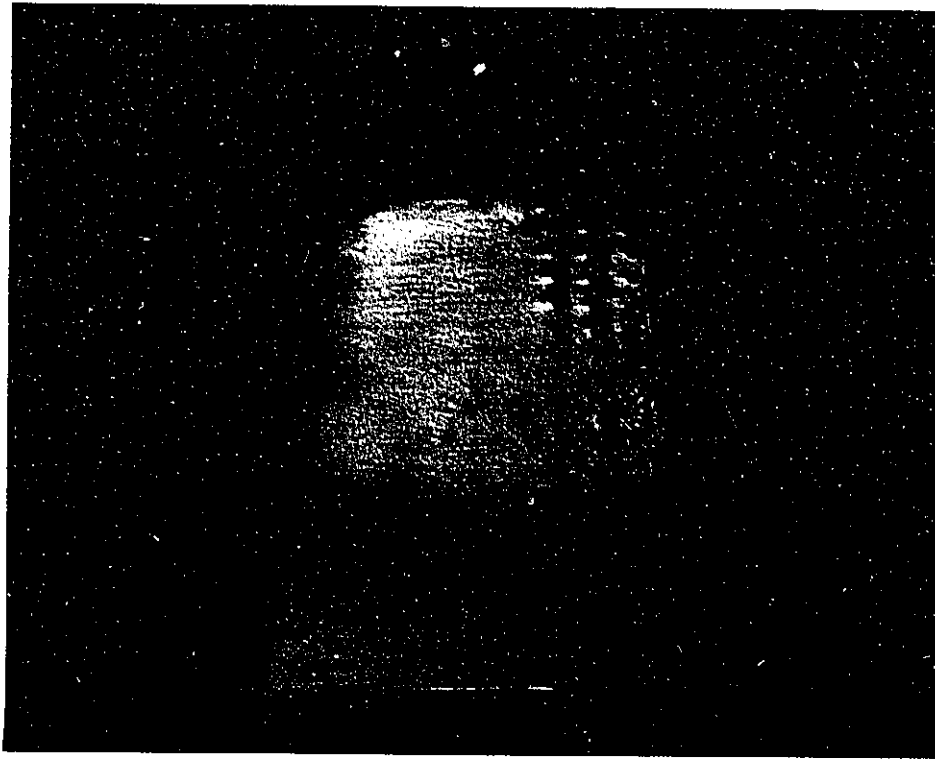


Figure 5. 1 mm aperture light source - off axis

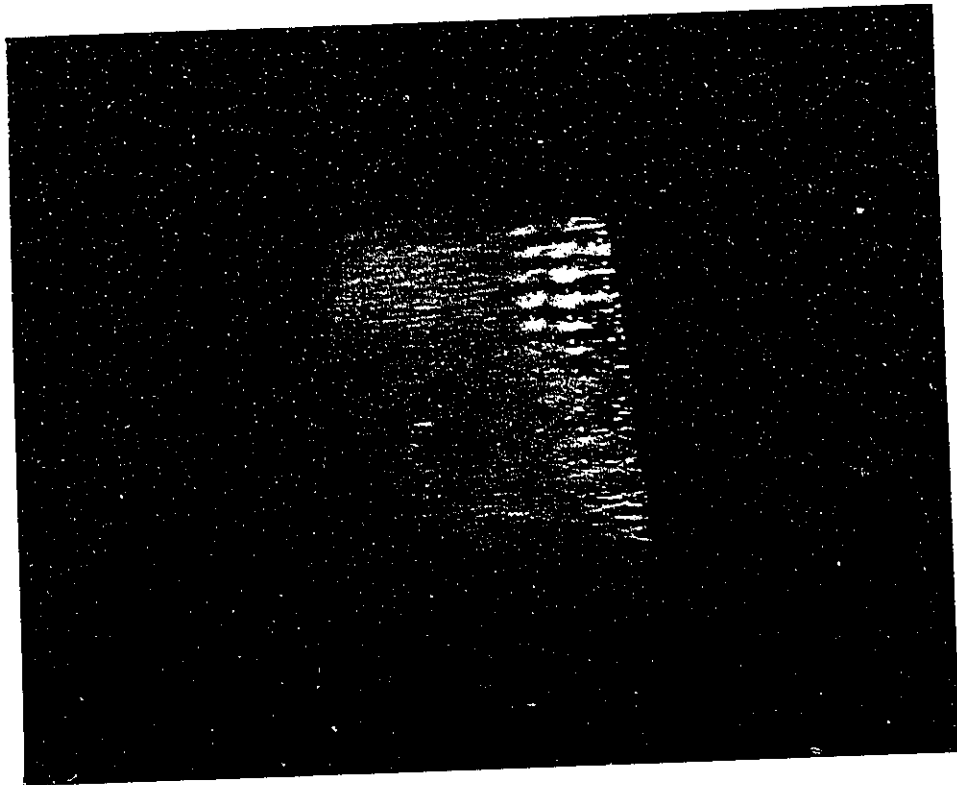


Figure 6. 5 mm aperture light source - off axis

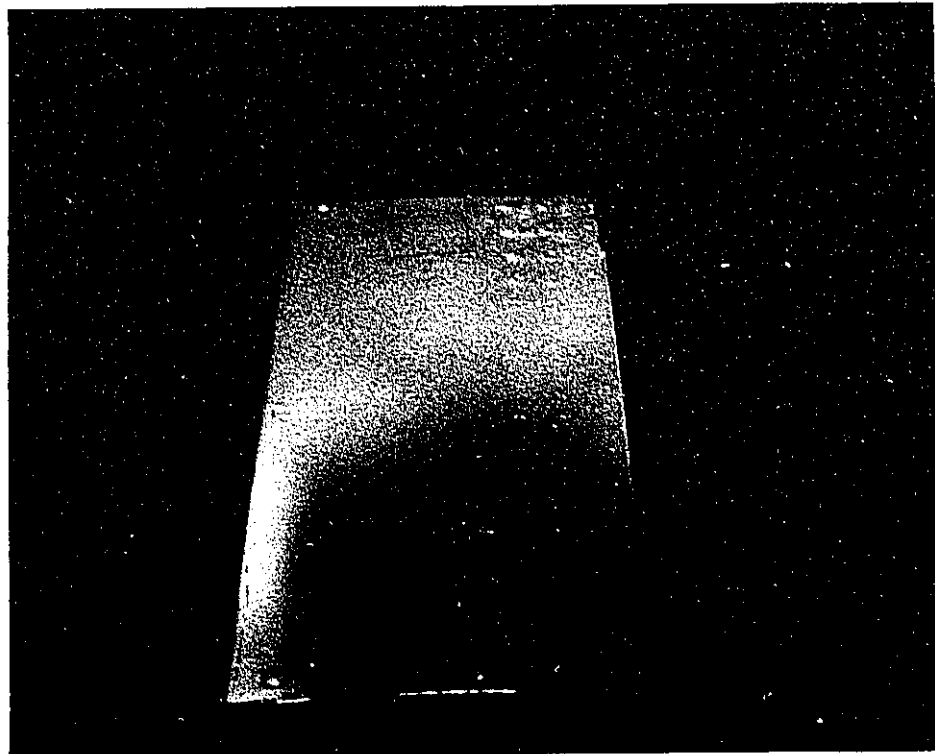


Figure 7. 25 mm aperture light source - off axis

3.2. Contour Measurements

3.2.1. Purpose

The purpose of this contour measurement was to evaluate the amplitude of the deformation of the outer skin and to generate the simulated actual shape of the pillowing using the data from this experiment.

3.2.2. Method

The arrangement of equipment used for contour measurements is shown schematically and photographically in Figure 8 and 9, respectively. Figure 10 is the closeup look of the LVDTs. The sample segment bounded by four rivets which had the most severe deformation (according to the D Sight image) was chosen to be measured. The dimension of this segment is 28 x 22 mm. As shown in Figure 8, LVDT1 (which measure the vertical Z displacement) was moved along the longer side of the surface of the segment using a motor driven slide. This horizontal X position was measured by LVDT2 attached to the motorized slide. The movement Y along the short side of the segment was adjusted manually in 1 mm increments. A Snap-Master data acquisition system using a Metrabyte A/D Board was used to simultaneously record the output from two LVDTs which is shown in Figure 11.

3.2.3. Results

The maximum deformation of the outer skin was 0.01164". The simulated actual shape of the deformed outer skin was generated using the LVDT data from this experiment and shown as Figure 12. The calibration constant for LVDT1 is 11.56 inches/V and the calibration constant for LVDT2 is 3.36 inches/V.

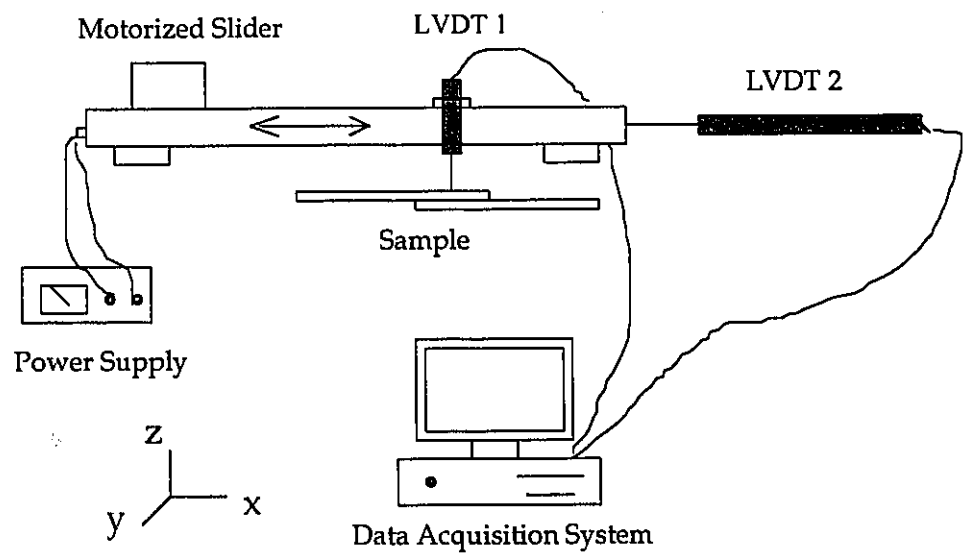


Figure 8. Schematic of LVDT setup

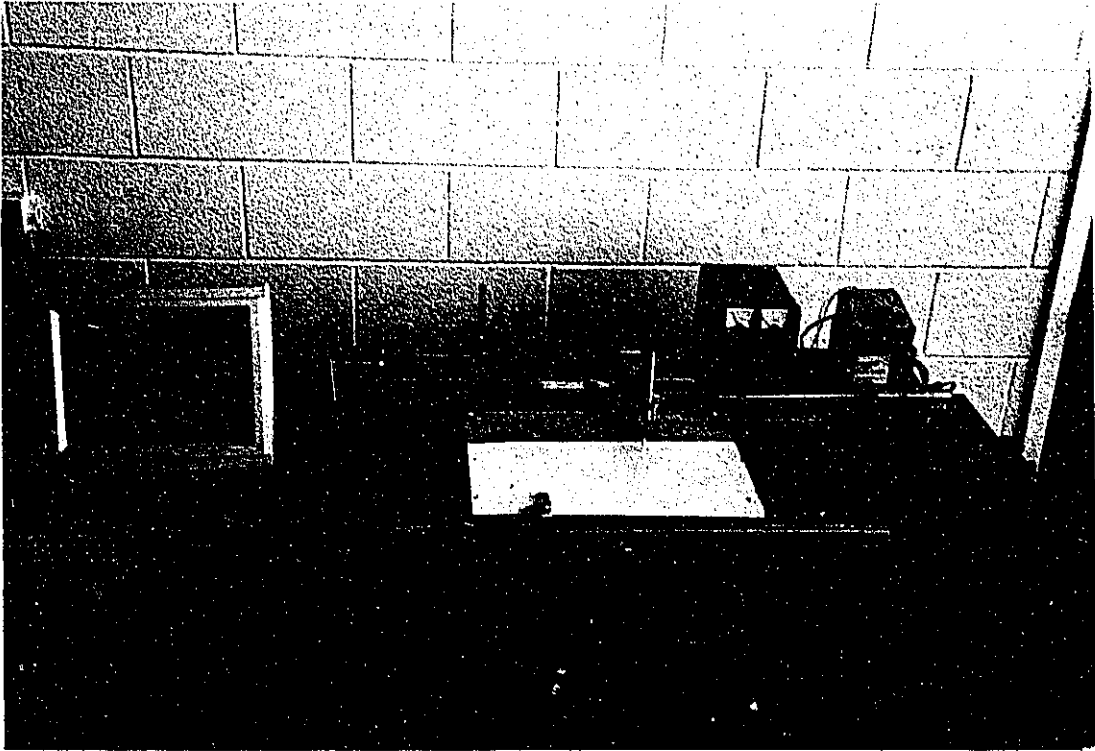


Figure 9. Photograph of LVDT setup

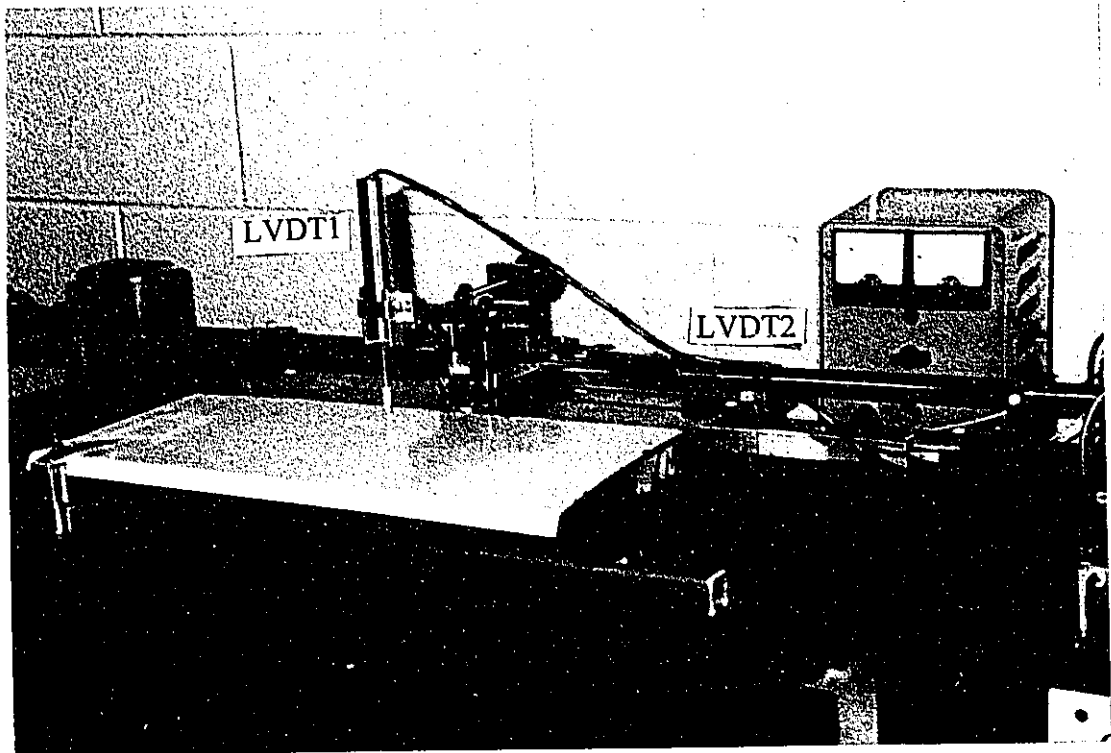


Figure 10. Close-up of the LVDTs

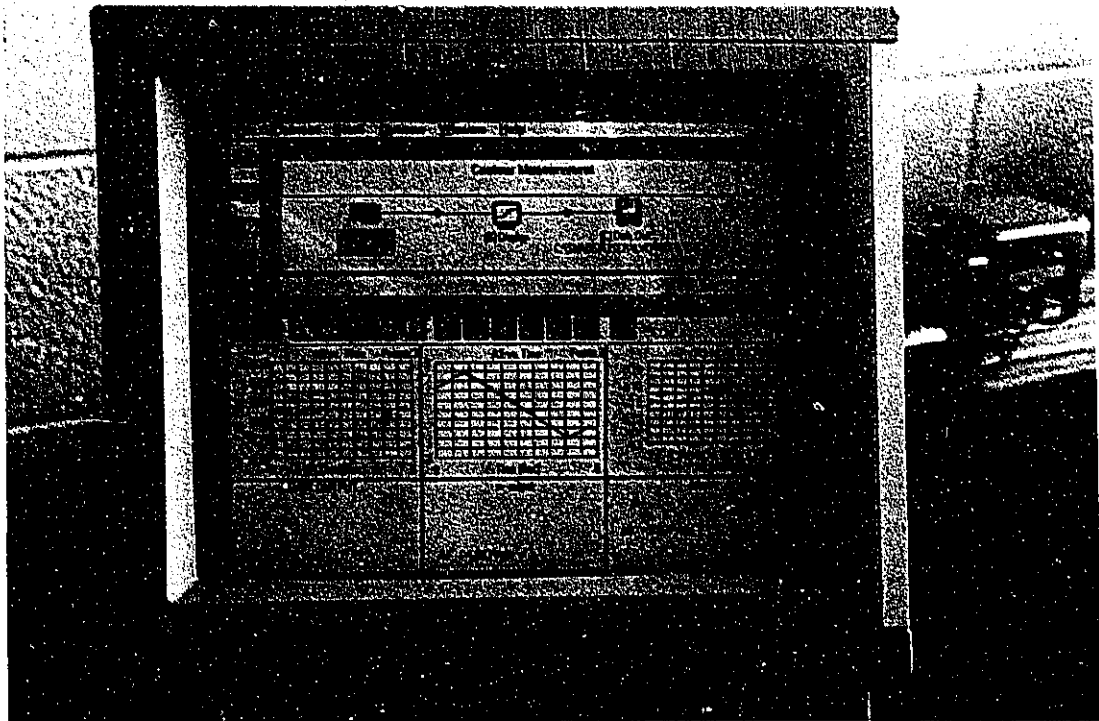


Figure 11. Computer results

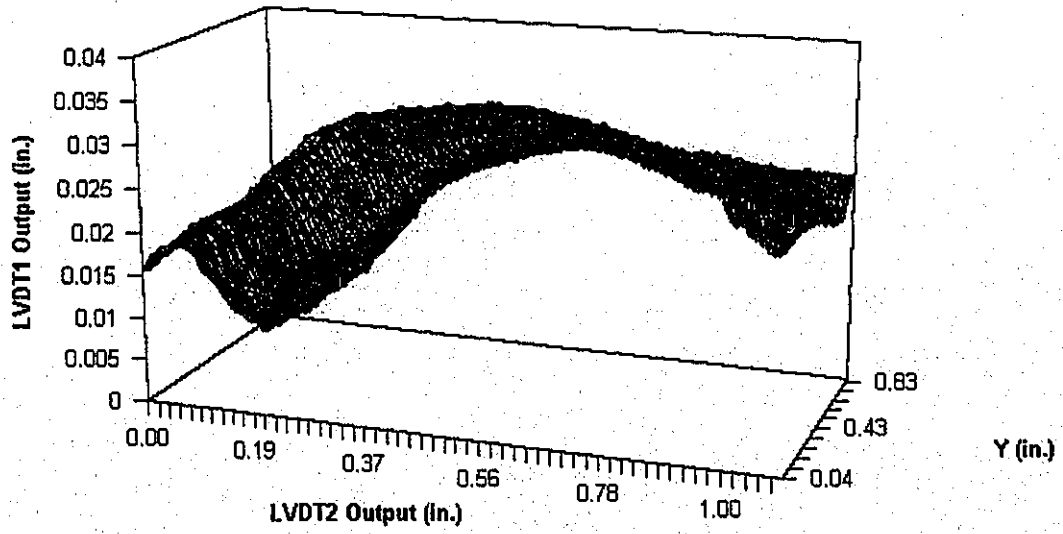


Figure 12. 3D plot of the LVDT data

3.3. Ultrasonic Inspection

3.3.1. Introduction to Ultrasonic Inspection

Ultrasonic nondestructive evaluation is a valuable technique for finding defects in aircraft structures. It can detect debonds, corrosion damage and cracks in various aircraft components.

A piezoelectric transducer generates acoustic energy and converts returned acoustic energy into electrical signals which can be processed to identify the reflector. The acoustic energy propagates through the component and is reflected by abrupt changes in modulus and/or density that can be caused by a defect. The amplitude of the electrical signals is related to the defect size and the time of flight of the signal provides depth information. Raster scanning a focused ultrasonic transducer over the part generates a high resolution image of the reflector which provides information such as shape, depth and density of the reflector. Planar views (C-scans) display size, shape, and location of the reflector in the x and y plane and cross-sectional view (B-scans) displays thickness of the reflector in the x or y and the z plane.

3.3.2. Method

In a newly developed ultrasonic method, an acoustic lens is employed to focus a high radio frequency pulse from a piezoelectric transducer in a liquid coupling medium (Figure 13). A wide-field pulse acoustic microscope with operation frequency of 50 MHz is used for visualization of a 2 mm diameter area. The lens is in the form of a spherical

cavity at the end of the sound guide. On interacting with the sample a focused beam is partially reflected from the sample and partially passes through it. In the former case a reflecting microscope was used; and in the latter case, after the beam passes through a second lens, a transmission acoustic microscope is used. Subsequent operations include the scanning of the sample relative to the local region, recording the signal at every point and storing the signal in a memory unit, synchronizing the sweep with the scanning, and using the signal to control the intensity of the electron beam. These operations result in the formation of an acoustic image on the display screen. The whole setup of this experiment is shown as Figure 14 and 15.

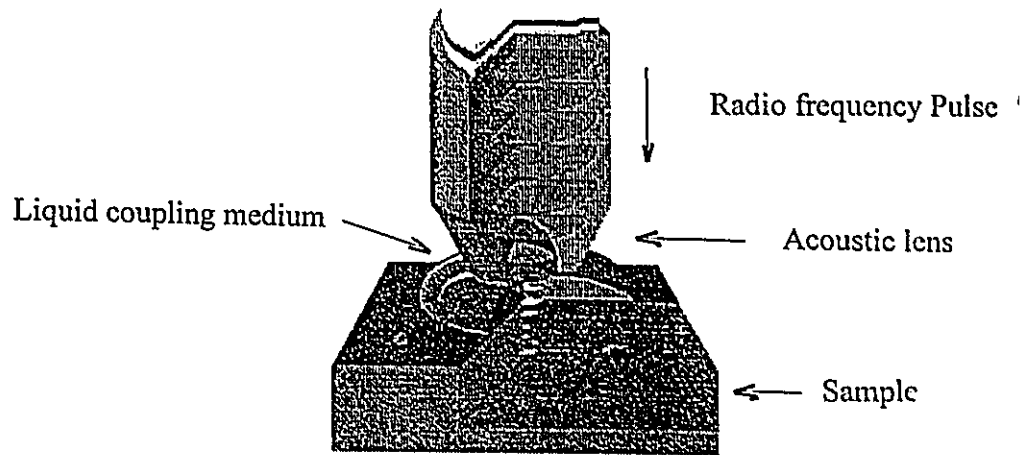


Figure 13. Schematic of ultrasonic transducer

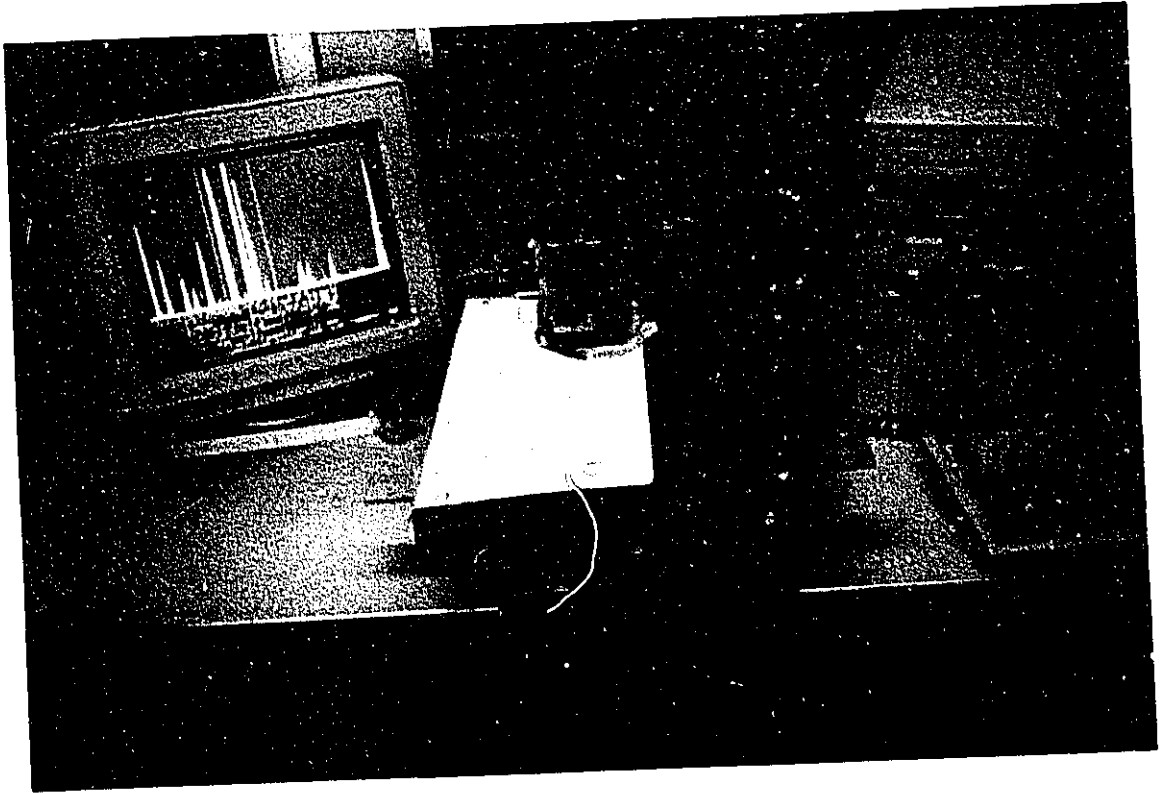


Figure 14. Photograph of ultrasonic setup

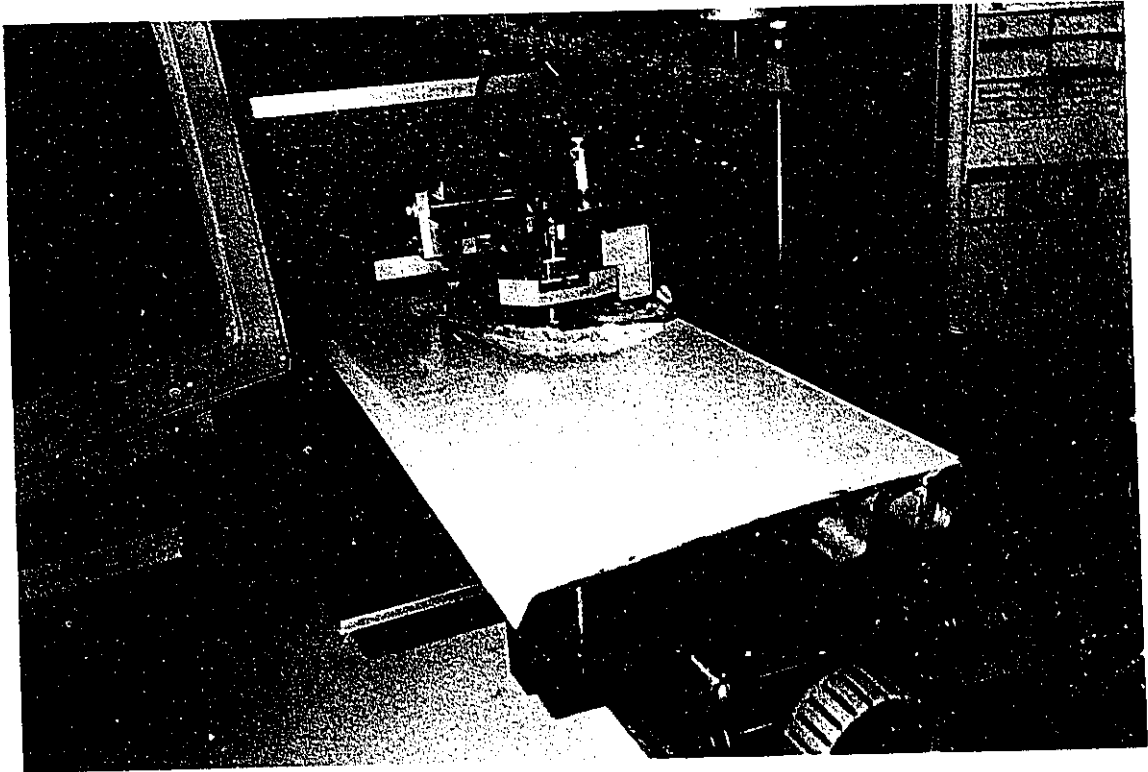


Figure 15. Close-up photograph of the ultrasonic test

3.3.3. Results

(Results courtesy of Dr. R.Maev)

The experiment was set up to show and find interlaminar corrosion.

An ultrasonic B-scan was generated as shown in Figure 16. In this cross-sectional view, the thickness of the top plate is represented by the black stripe. This has insufficient resolution to measure thickness.

Figure 17 is an ultrasonic C-scan. By this planar view, the interlaminar corrosion area was found around the rivet.

Sections of the sample with severe corrosion, light corrosion and without corrosion are shown in Figure 18, 19, and 20, respectively.

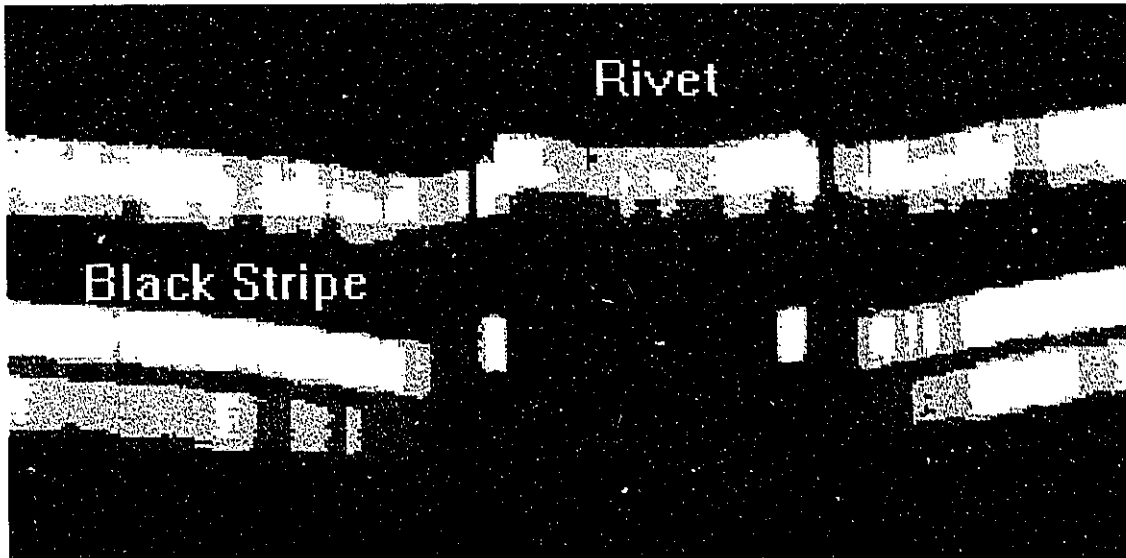


Figure 16. Ultrasonic B-scan



Figure 17. C-scan showing interlaminar corrosion at a rivet

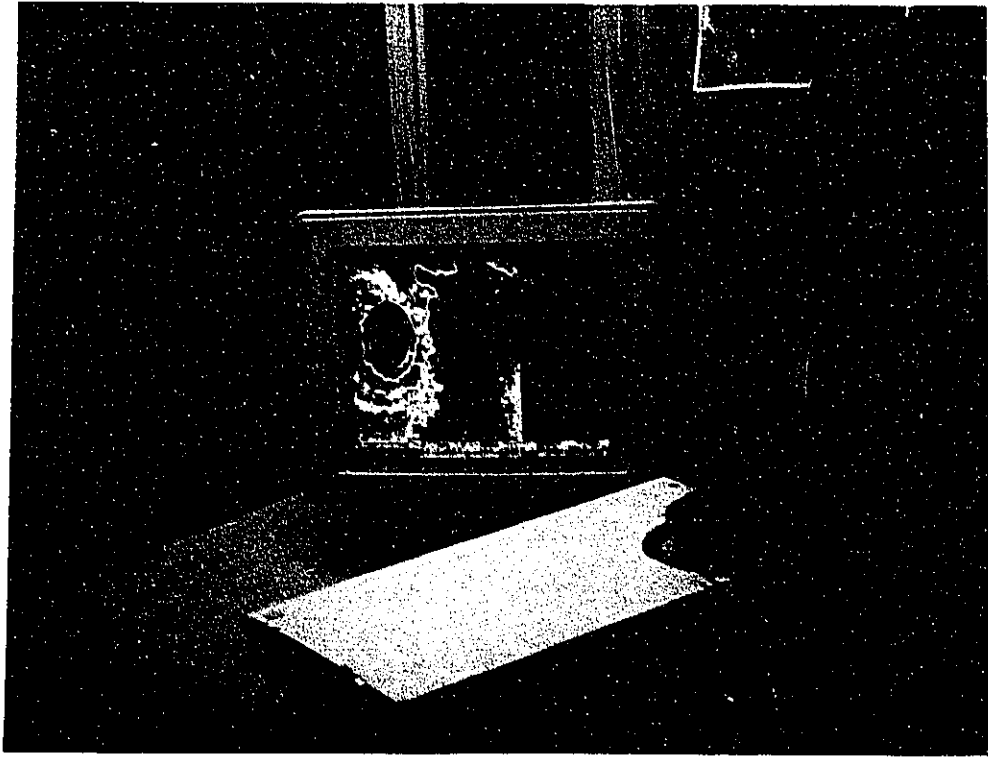


Figure 18. Photograph of rivet with severe corrosion

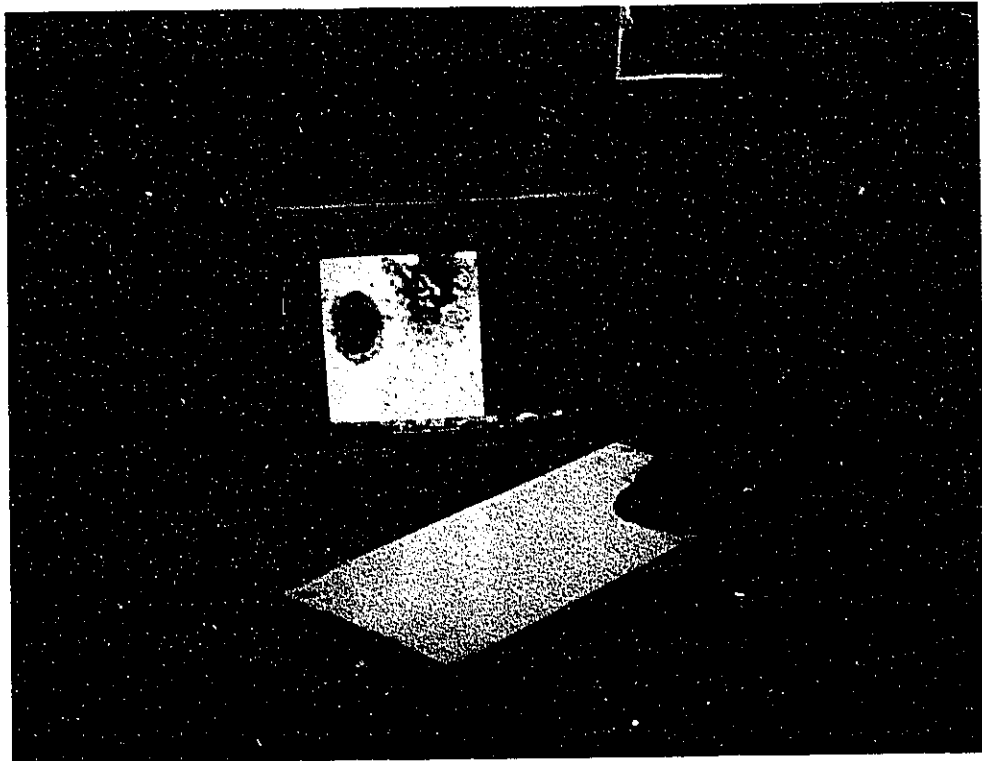


Figure 19. Photograph of rivet with light corrosion

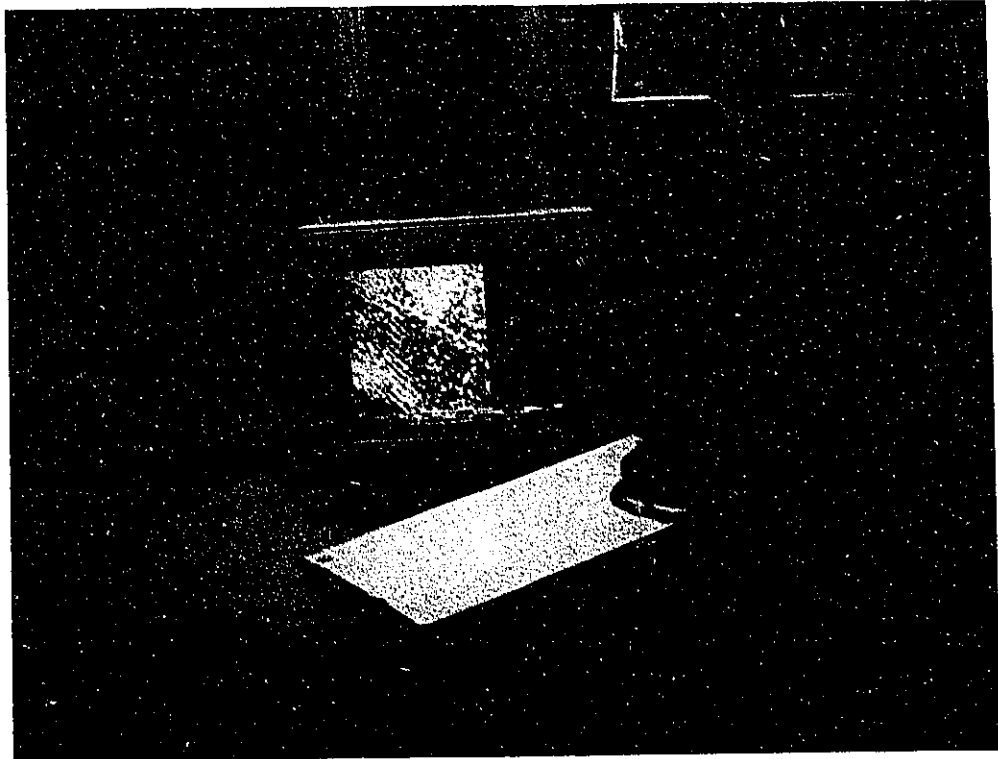


Figure 20. Photograph of rivet without corrosion

CHAPTER 4

MATHEMATICAL MODEL

4.1. Purpose

The theoretical solution from an analytical model of the pillowing in fuselage joints would provide a correlation for FEA results.

4.2. Method

This model was developed on the premise that after the lap joint disbonds, assuming the surfaces were initially bonded, the aircraft skin between the rivets deforms perpendicularly to the lap joint surface, creating space within the joint to accommodate the additional volume required by the corrosion product.

The model initially assumes that the product of corrosion is distributed within the joint so as to exert a uniform lateral pressure on the fuselage skins. It was also assumed that this joint was symmetrical about its mid-plane. Thus, only the outer skin of the lap joint would be modeled.

The closed-form classical plate theory of Timoshenko and Krieger⁸ was used to calculate the deformation of the outer skin supported by equidistant rivets and subject to uniform pressure.

According to this plate theory, if the dimensions of the plate are large in comparison with distances a and b between the columns (as shown in Figure 21) and the lateral load is uniformly distributed, it can be concluded that the bending in all panels, which are not close to the boundary of the plate, may be assumed to be identical, so that the problem can be limited to the bending of one panel only.

Taking the coordinate axes parallel to the rows of rivets and the origin at the center of a panel, we may consider this panel as a uniformly loaded rectangular plate with sides a and b . From symmetry we conclude that the deflection surface of the plate is as shown by the dashed lines in Figure 21(b). The maximum deflection is at the center of the plate, and the deflection at the corners is zero.

To simplify the problem, it is assumed that the cross-sectional dimensions of the rivets are small and can be neglected in so far as deflection and moments at the center of the plate are concerned.

As a uniformly loaded rectangular plate supported at the corners, it is concluded from symmetry that the slope of the deflection surface in the direction of the normal to the boundary and the shearing force are zero at all points along the edges of the plate except at the corners.

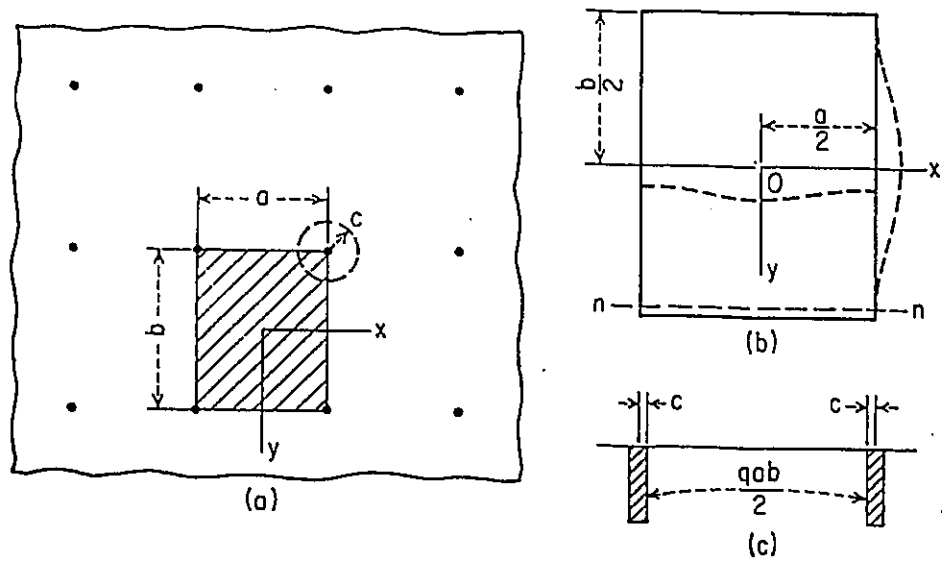


Figure 21. Mathematical model - plate

4.3. Results

The following equation is the basic plate equation and any expression for displacement w that satisfies this equation is a solution of a plate problem.

$$\frac{\partial^4 w}{\partial x^4} + 2 \frac{\partial^4 w}{\partial x^2 \partial y^2} + \frac{\partial^4 w}{\partial y^4} = \frac{q}{D} \quad (1)$$

where q = pressure

$$D = Eh^3 / [12(1-\nu^2)]$$

and h = thickness.

This equation can also be written in the symbolic form

$$\Delta \Delta w = \frac{q}{D} \quad (2)$$

where

$$\Delta w = \frac{\partial^2 w}{\partial x^2} + \frac{\partial^2 w}{\partial y^2} \quad (3)$$

The total deflection w is assumed to be an infinite series of the form

$$w = w_1 + w_2 \quad (4)$$

where

$$w_1 = \frac{qb^4}{384D} \left(1 - \frac{4y^2}{b^2}\right)^2 \quad (5)$$

represents the deflection of a uniformly loaded strip clamped at the ends $y = \pm b/2$ and satisfies the differential equation (1) of the plate as well as the boundary conditions

$$\begin{aligned} \left(\frac{\partial w_1}{\partial x}\right)_{x=\pm a/2} &= 0, \\ (Q_x)_{x=\pm a/2} &= -D \frac{\partial}{\partial x} \left(\frac{\partial^2 w_1}{\partial x^2} + \frac{\partial^2 w_1}{\partial y^2} \right)_{x=\pm a/2} = 0 \end{aligned} \quad (6)$$

where Q_x = shearing force.

The deflection w_2 is taken in the form of the series

$$w_2 = A_0 + \sum_{m=2,4,6,\dots}^{\infty} Y_m \cos \frac{m\pi x}{a} \quad (7)$$

each term of which satisfies the conditions (6). The functions Y_m must be chosen so as to satisfy the homogeneous equation

$$\Delta\Delta w_2 = 0 \quad (8)$$

and so as to make w satisfy the boundary conditions at the edges $y = \pm b/2$. Equation (8) and the conditions of symmetry are satisfied by taking series (7) in the form

$$w_2 = A_0 + \sum_{m=2,4,6,\dots}^{\infty} \left(A_m \cosh \frac{m\pi x}{a} + B_m \frac{m\pi y}{a} \sinh \frac{m\pi y}{a} \right) \cos \frac{m\pi x}{a} \quad (9)$$

where the constants A_0 , A_m , and B_m are to be determined from the boundary conditions along the edge $y = b/2$. From the condition concerning the slope, viz., that

$$\left(\frac{\partial w}{\partial y} \right)_{y=b/2} = \left(\frac{\partial w_1}{\partial y} + \frac{\partial w_2}{\partial y} \right)_{y=b/2} = 0 \quad (10)$$

Considering the boundary condition concerning the shearing force, it is seen that on a normal section mn (Fig. 21b) of the plate infinitely close to the boundary $y = b/2$, the shearing force Q_y is equal to zero at all points except those which are close to the rivet, and at these points Q_y must be infinitely large in order to transmit $1/2$ the finite load to each rivet (Fig. 21c) along an infinitely small distance between $x = a/2 - c$ and $x = a/2 + c$. The required boundary condition is taken in the following form:

$$\begin{aligned} (Q_y)_{y=b/2} &= -D \left(\frac{\partial^3 w}{\partial y^3} + \frac{\partial^3 w}{\partial x^2 \partial y} \right)_{y=b/2} \\ &= -\frac{P}{a} \sum_{m=2,4,6,\dots}^{\infty} (-1)^{m/2} \cos\left(\frac{m\pi x}{a}\right) - \frac{P}{2a} \end{aligned} \quad (11)$$

where $P = qab$ is the total load on one panel of the plate.

On account of the boundary condition $(\partial w / \partial y)_{x=\pm a/2} = 0$, the following constants are obtained:

$$\begin{aligned} A_o &= \frac{qb^4}{D} a_o, \\ A_m &= \frac{qb^4}{D} a_m, \\ B_m &= \frac{qb^4}{D} b_m \end{aligned} \quad (12)$$

where

$$a_o = - \frac{a^3}{2\pi^3 b^3} \sum_{m=2,4,6,\dots}^{\infty} \frac{1}{m^3} \left(\alpha_m - \frac{\alpha_m + \tanh \alpha_m}{\tanh^2 \alpha_m} \right) \quad (13)$$

and

$$a_m = - \frac{a^3}{2m^3 \pi^3 b^3} (-1)^{m/2} \frac{\alpha_m + \tanh \alpha_m}{\sinh \alpha_m \tanh \alpha_m} \quad (14)$$

where

$$\alpha_m = \frac{m\pi b}{2a} \quad (15)$$

and

$$b_m = \frac{a^3}{2m^3\pi^3b^3} (-1)^{m/2} \frac{1}{\sinh \alpha_m} \quad (16)$$

Substituting the above expressions to the equation (4), the deflection at any point of the plate can be calculated. The maximum deflection is evidently at the center of the plate, it is given as:

$$(w)_{x=0, y=0} = \frac{qb^4}{D} \left(\frac{1}{384} + \alpha_0 + \sum_{m=2,4,6,\dots}^{\infty} \alpha_m \right) \quad (17)$$

Concentrated reactions are acting at the points of support of the plate, and the moments calculated from the above equation become infinitely large. So it is assumed that the reactive forces are distributed uniformly over the area of a circle representing the cross section of the rivet. The bending moments per unit width arising at the center of the supporting area remain finite in such a case and it can be expressed as follows for a square plate ($a = b$):

$$\begin{aligned} (M_x)_{x=y=a/2} &= (M_y)_{x=y=a/2} \\ &= -\frac{qab}{4\pi} (1+\nu) \left(\log \frac{a}{c} - 0.811 \right) \end{aligned} \quad (18)$$

and the bending moments corresponding to the centers of columns of rectangular cross section also can be calculated by assuming that the reactions are uniformly distributed over the rectangles, shown shaded in Fig.22, which represent the cross sections of the rivets.

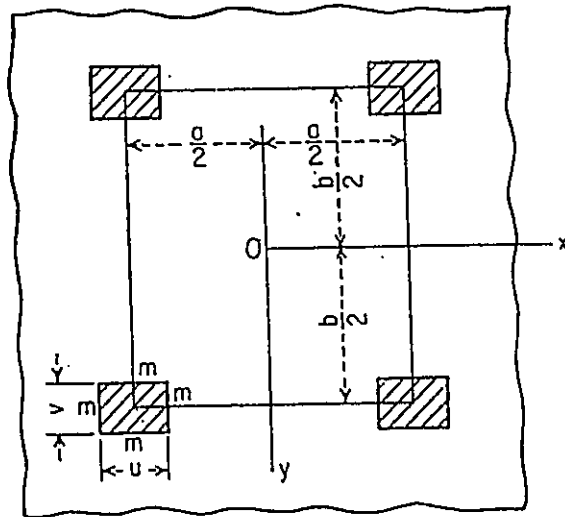


Figure 22. Mathematical model - segment.

The moments per unit width at the centers of the panels are given by the following formulas:

$$\begin{aligned}
 (M_x)_{x=y=0} &= (M_y)_{x=y=0} \\
 &= -\frac{(1+\nu)qa^2}{4} \left(\frac{1-k^2}{12} + \frac{1}{\pi^3 k^2} \sum_{m=1}^{\infty} (-1)^{m+1} \frac{\sinh m \pi k \sin m \pi k}{m^3 \sinh m \pi} \right)
 \end{aligned} \tag{19}$$

where $k = c/(0.57a)$, c denotes the radius of the rivet column as shown in Figure 21.

The maximum principal stress is given as:

$$\begin{aligned}
 (\sigma_x)_{\max} &= \frac{6M_x}{h^2}, \\
 (\sigma_y)_{\max} &= \frac{6M_y}{h^2}
 \end{aligned} \tag{20}$$

where h = plate thickness.

The Von Mises stress is:

$$\text{Von Mises Stress} = \sqrt{\frac{1}{2}[(\sigma_1 - \sigma_2)^2 + (\sigma_2 - \sigma_3)^2 + (\sigma_1 - \sigma_3)^2]} \tag{21}$$

$$\text{where } \sigma_1 = \pm \sigma_{x\max},$$

$$\sigma_2 = \pm \sigma_{y\max},$$

$$\sigma_3 = 0, \text{ or } -P.$$

CHAPTER 5

FINITE ELEMENT STRESS ANALYSIS

5.1. Purpose

The purpose of the Finite Element Analysis (FEA) was to correlate the amplitude of the pillowing deformation of the outer skin of the lap joint to the magnitude of the flexure stress superposed on the design as a result of the corrosion driven phenomenon.

5.2. Method

The Finite Element Analysis was conducted using Algor Static Stress Analysis. SuperDraw II was used to enter two or three dimensional geometry of the plate and to create the mesh. The Decoder was used to enter the material properties, (see Table 1), plate elements and brick elements were chosen respectively. Several runs modeling the whole and quarter plate were conducted to determine the sensitivity of the system to the mesh density (i.e. the number of elements)

5.2.1. Whole Plate Model

The actual lap joint, shown in Figure 23, contain free edges (and stiffeners) and the deformation of the outer skin was supported by equidistant rivets . The plate segment

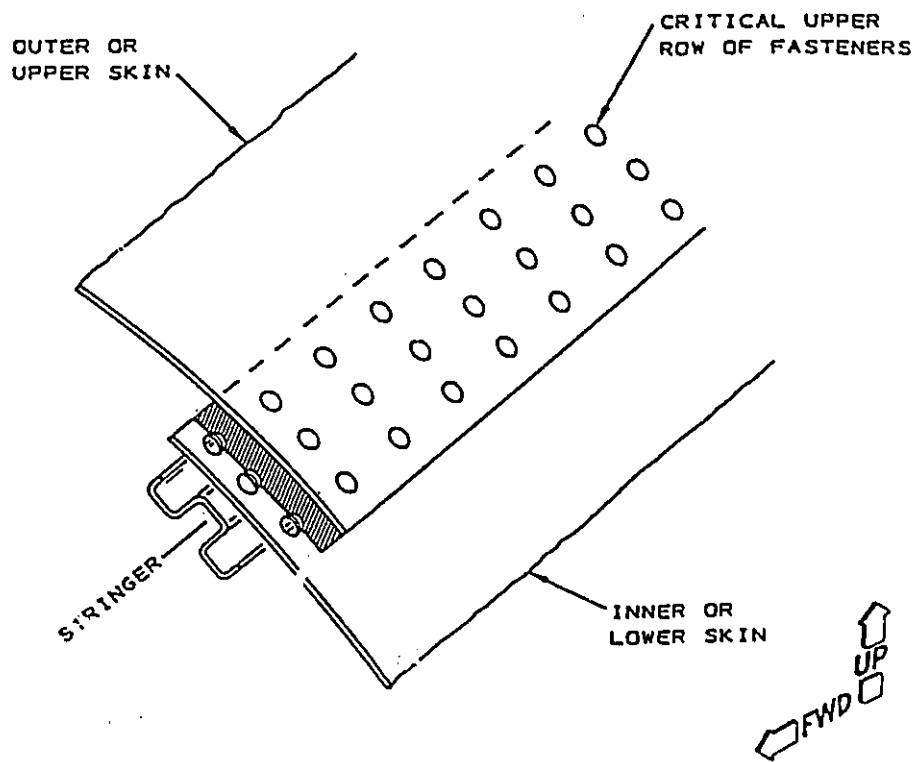


Figure 23. Schematic of an actual lap joint

Table 1: Material properties used in FEA models

Property	Value
Young's Modulus	10.5×10^6 psi
Poisson's Ratio	0.3
Thickness	0.0800"
Material	Aluminum Alloy 2024-T4

bounded by four rivets was modeled and the deflections in this area (the shaded area in Fig.21a) were assumed to be representative of the entire plate and subjected to a uniform lateral pressure.

5.2.2. Quarter Plate (Brick) Model

Since the segment of the plate (bounded by four rivets) and its boundary conditions are symmetric about X and Y center lines (axes), only one quarter of the plate has to be modeled and proper symmetry boundary conditions applied to the center lines. A symmetry boundary condition is where the plate is reflected, as a mirror, about that axis. The values are equal at equal locations on either side of a symmetric boundary.

As shown in Figure 24 different boundary conditions were placed along four edges of the quarter plate. A constant lateral pressure ($p = 1000$ psi) was applied normal to the surface of the plate .

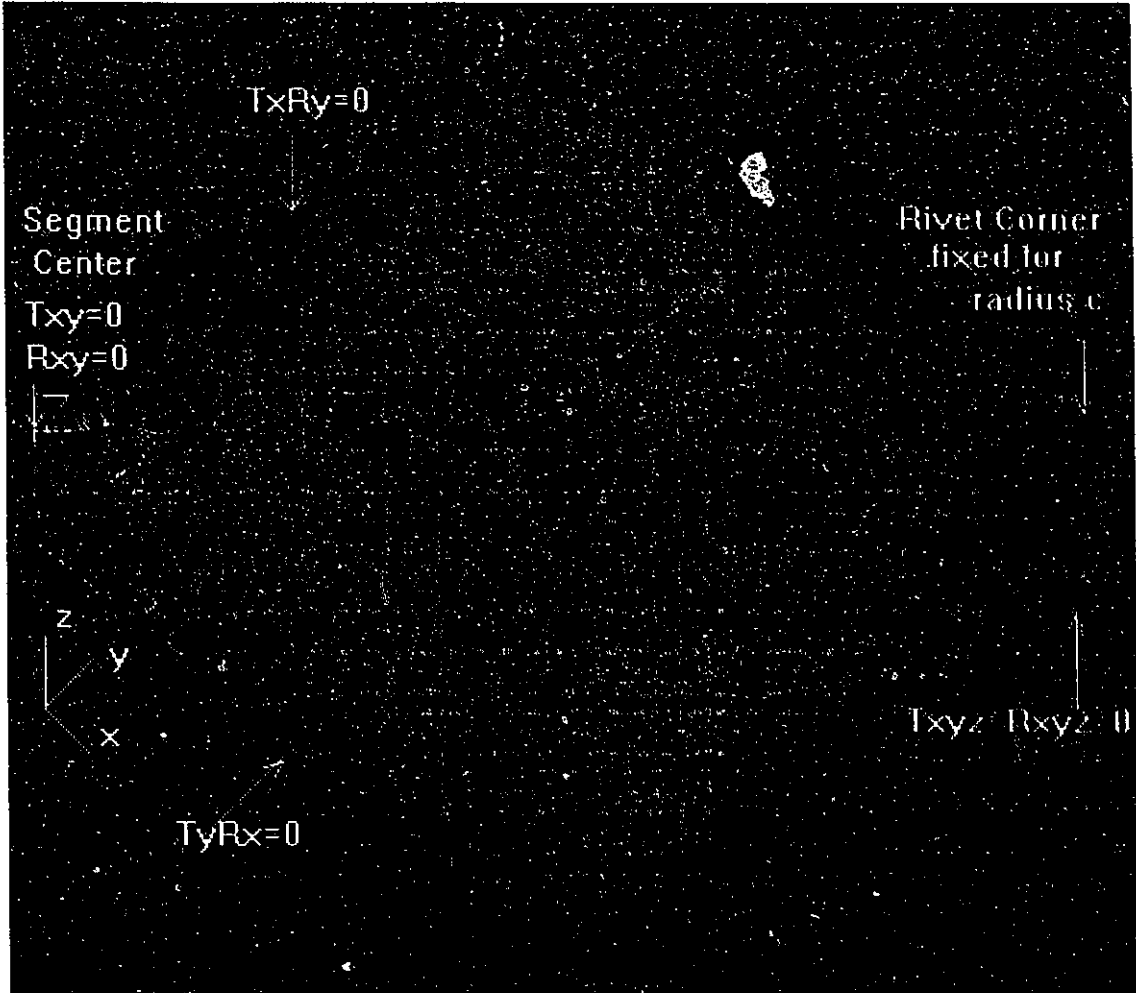


Figure 24. FEA boundary conditions of quarter plate

The corner of the segment has all six boundary conditions fixed (i.e. no translation, no rotation) for a radius $c = 0.018$ " inches.

The term t_x , t_y , and t_z refer to translation of the node in the direction specified and r_x , r_y , and r_z refer to rotation at that node about the specified axis. If an individual term is equal to 0, it indicates a condition that is restrained, otherwise it is free to translate or rotate.

Two finite element models were generated to determine the accuracy of using 2-D plate elements and 3-D brick elements to model the out-of-plane displacements. The mesh size was refined to determine the effect that element size has on the accuracy of the results.

The maximum displacement ($w_{x=0,y=0}$ Fig.21) of the segment for the various mesh densities are given in Table 2.

Table 2. Maximum Displacement for various mesh densities for $a = b = 1$ in. and pressure = 1000 psi..

Whole Plate Plate Elements	Mesh	Quarter Plate Brick Element	Mesh
0.00892	10x10x1	0.01066	10x10x4
0.0099	20x20x1	0.01162	20x20x4
0.01038	30x30x1	0.01169	30x30x4
0.01105	60x60x1	-----	-----
0.01178	Theoretical	0.01178	Theoretical

5.3. Results

5.3.1. Mesh Density

At the rivet point the stress value is more sensitive to the number of elements. When the stress is analyzed, it is more important to have a denser mesh.

The processing time increased dramatically as the mesh density was increased, and there is a practical limit to how many elements could be modeled. When a model more than 60x60x1 plate elements (30x30x4 brick elements) was attempted, the computer with 110 Megabytes of free space ran out of hard disk space.

Since the change in displacement of the center of the segment was small between 20x20x4 and 30x30x4 elements when brick elements were used, it was decided that 20x20x4 brick elements would be sufficient to model this plate.

From this study, it was concluded that the 3-D brick elements could provide more accurate results than 2-D plate elements. Therefore, a 3-D brick element with 20x20x4 elements wide was used to evaluate the magnitude of the flexure stress of the deformed outer skin.

5.3.2. Stress Analysis

Table 3 shows a comparison of the Von Mises Stress at the center ($x=0,y=0$) and the corner ($x=a/2,y=b/2$) of the segment obtained from theoretical and FEA analysis.

Table 3. Theoretical and FEA results

	σ_{center} (psi)	σ_{corner} (psi)
Theoretical	33600	128,000
FEA (Von Mises)	33900	175,000

The Von Mises Stress through the thickness of the segment from the top ($z=0$) to the bottom ($z=0.08$ ") at 0.02" intervals are shown as Table 4:

Table 4. Von Mises stress profile through the plate thickness

z Position	σ_{center} (psi)	σ_{corner} (psi)
0"	50000	170000
0.02"	26400	178000
0.04"	17000	178000
0.06"	26200	178000
0.08"	49800	170000

Since the yield strength for Aluminum Alloys 2024-T4 is 48 kpsi, the above results indicate that the outer skin of this segment is significantly past the yield condition in the corners and at the yield condition in the centers. The entire plate then is in the plastic

condition. It is highly likely that any cyclic live load superposed on this fully yielded condition will result in cracks which are propagated by the live cyclic stress. If we were given permission to dismantle this specimen, micro cracks would likely be found in the area of the rivets.

The out-of-plane displacement contour plot and stress distribution are shown in Figure 25 and 26 respectively.

As can be seen from those figures, the maximum displacement occurs at the center of the segment, and the maximum Von Mises stress occurs in the vicinity of the rivet.

From the results obtained from Algor, it was seen that the good agreement is obtained between FEA and theoretical results and that the FEA method provides more information which couldn't be obtained from the formulas in the mathematical model.

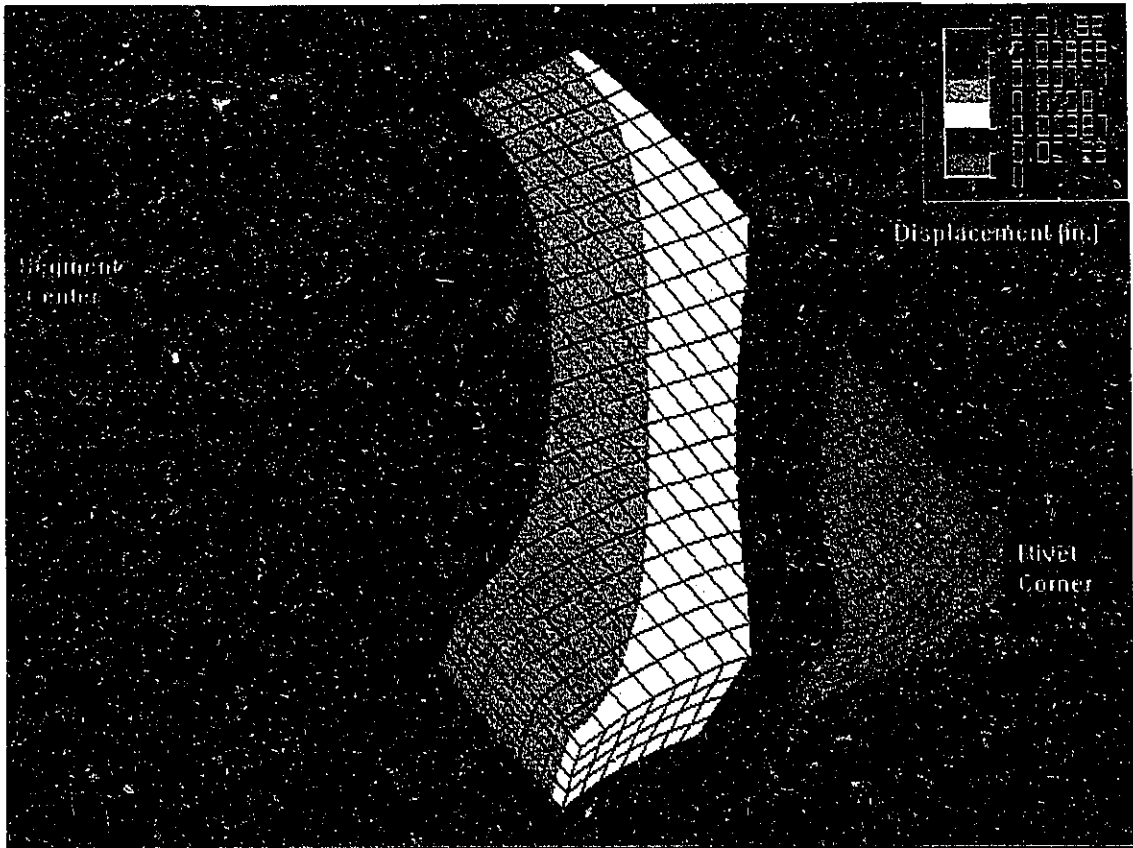


Figure 25. FEA displacement of a quarter plate model

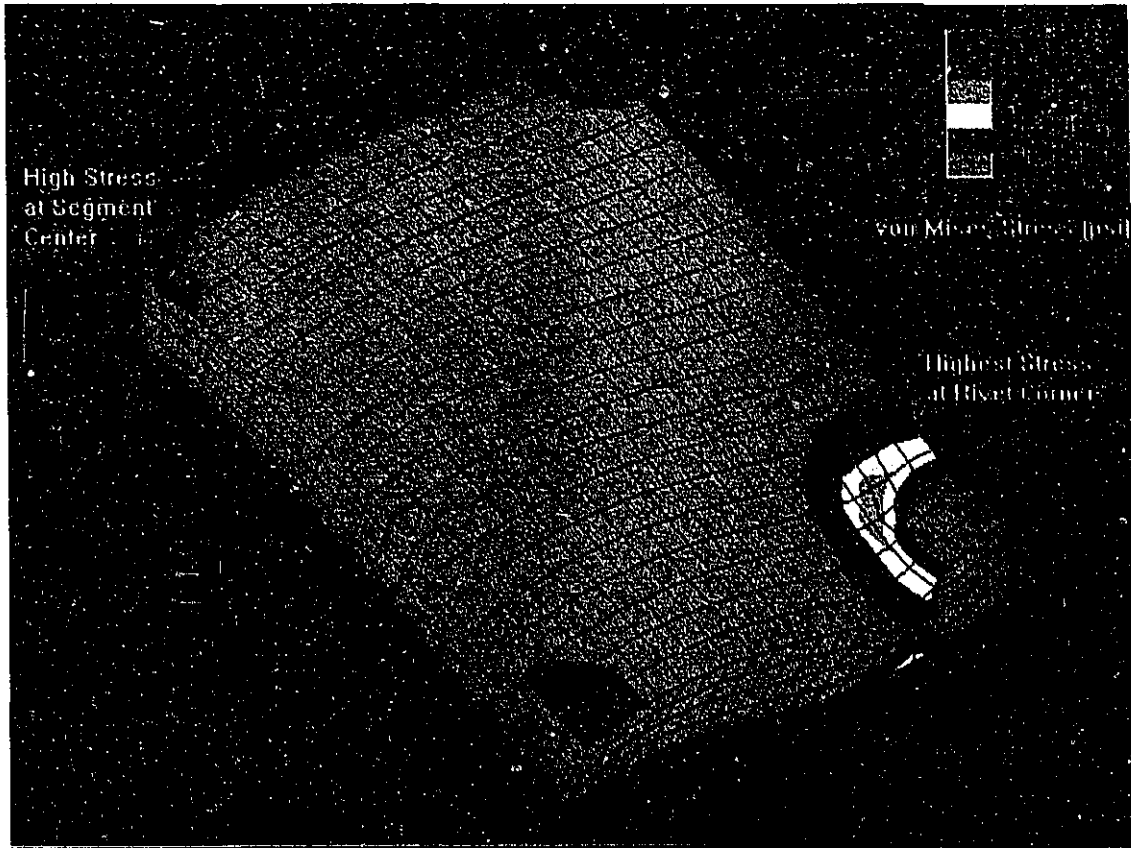


Figure 26. FEA stress distribution of quarter plate model

CHAPTER 6

CONCLUSIONS

The following conclusions can be made from the present work:

1. D Sight is inexpensive, fast, easy to use and gives full field results. Its results are also well corroborated by LVDT mapping of the pillowing deformation caused by corrosion build-up. D Sight would be ideal for corrosion monitoring in the large area of an aircraft fuselage.

2. While the D Sight results are mainly qualitative, the application of the LVDT contour measurement facilitates quantitative interpretation of the effect of corrosion build-up.

3. A new Ultrasonic Detection Method developed by R.Maev shows the applicability of his technique to identify (show or find) interlaminar corrosion. However in the format used here, there was insufficient resolution to detect a change in the skin thickness as a result of the corrosion present.

4. Good agreement has been obtained between the finite element technique using 3D brick elements and the mathematical model. The theoretical method provided confidence in the FEA results.

5. The analysis shows that the pillowing results in stress far in excess of the yield strength of the aluminum material. Any live cyclic strain superposed on this condition would likely result in crack propagation in the fuselage lap joints. These cracks will start in the vicinity of the rivets where the stress and strain are highest.

CHAPTER 7

RECOMMENDATIONS

From the conclusions made from the present work, the following suggestions are proposed for the future work:

1. Further work needs to be done to determine the effect that a stiffener has on the pillowing displacements in a lap joint.

2. Actual lap joints have to be torn down and visual inspection used to obtain conclusive verification of ultrasonic corrosion monitoring. Dismantling would also confirm that the pillowing detected by D Sight was due to interlaminar corrosion products. It would also show if the panel analyzed had in fact yielded and/or if micro cracks are present in the vicinity of the rivets.

3. A data base of measured pillowing displacements of the same lap joints with different service age are required to develop a retrospective correlation between the pillowing deformation and aircraft service life.

4. Comparative studies between D Sight and LVDT mapping would be useful for the development and verification of a mathematical model for the quantitative interpretation of D Sight results.

REFERENCES

1. **AGARD**(Advisory Group for Aerospace Research & Development), "Corrosion Detection and Management of Advanced Airframe Materials", Paper presented at the 79th Meeting of the AGARD Structures and Materials Panel on "Corrosion Detection and Management of Advanced Airframe Materials", (October 1994).
2. **D. A. Clark, R. L. Reynolds and T. R. Pryor**, "Panel Surface Flaw Inspection", U.S. Patent, No. 4,629,319, held by Diffracto Ltd. (Dec. 16, 1986).
3. **J. P. Komorowski, R. W. Gould, and W. J. Pastorius**, "A Technique for Rapid Inspection of Composite Aircraft Structure for Impact Damage" in "The Impact of Engineering NDI Methods on Aircraft Design, Manufacture and Maintenance," AGARD CP-462, (May 1990).
4. **J. P. Komorowski, D. L. Simpson, and R. W. Gould**, "Enhanced Visual Technique for Rapid Inspection of Aircraft Structures", Materials Evaluation, pp.1486-1490, (December 1991).
5. **J. P. Komorowski, R. W. Gould, A. Marincak, and S. Krishnakumar**, "Application of D Sight For Corrosion Detection in Fuselage Lap and Butt Joints", Report No. LTR-ST-1960, Institute for Aerospace Research, National Research Council of Canada, (January 1994).

6. **N. C. Bellinger, S. Krishnakumar, and J. P. Komorowshi**, " Modeling of Pillowing due to Corrosion in Fuselage Lap Joints", Canadian Aeronautics and Space Journal, Vol.40, No.3, pp.125-130, (September 1994).
7. **U.S. Department of Transportation**, (Federal Aviation Administration Technical Center), " National Aging Aircraft Research Program Plan", (October 1993).
8. **S. Timoshenko, S. Woinowsky-Krieger**," Theory of Plates and Shells", Second Edition, McGraw-Hill Book Company, (1959).
9. **R. L. Reynolds and O. L. Hageniers**, "A Rigorous Optical Theory of the DSIGHT Phenomenon", SPIE, Vol. 1332, pp.85-96, (1990).
10. **R. L. Reynolds, F. Karpala, D. A. Clarke, and O. L. Hageniers**, "Theory and Applications of A Surface Inspection Technique Using Double-Pass Retroreflection", Optical Engineering, Vol.32, No.9, pp.2122-2129, (September 1993).
11. **O.L. Hageniers**, "DSIGHT for large area aircraft inspection", SPIE, Vol.2001, pp.248-256, (1993).
12. **R. L. Reynolds, and O. L. Hageniers**, " Optical Enhancement of Surface Contour Variations for Sheet Metal and Plastic Panel Inspection", SPIE 964, pp.208-216, (1988).
13. **S. Krishnakumar, J. P. Komorowski, and I. Sproule**, "Chemical Characterization of Corrosion Products in Fuselage Lap Joints", Report No. LTR-ST-1952, Institute for Aerospace Research, National Research Council of Canada,

(November 1993).

14. **H. H. Uhlig, and R. W. Revie**, " Corrosion and Corrosion Control", John Wiley and Sons, New York, (1971).
15. **U. R. Evans**, " The Corrosion and Oxidation of Metals: Scientific Principles and Practical Applications:", Edward Arnold (Publishers) Ltd., London, (1960).
16. **R. G. Maev**, " Archives of Acoustics", Polish Scientific Publishers, Vol.13, No.1-2, (1988).
17. **G. H. Thomas, S. Benson, and S. Crawford**, " Three Dimensional Ultrasonic Imaging: An Aging Aircraft Nondestructive Inspection Tool", Nondestructive Inspection of Aging Aircraft, SPIE Vol.2001, (1993).
18. **D. K. Hsu, and T. C. Patton**, "Fatigue Induce Disbonds in Adhesive Lap Splices of Aluminum and Their Ultrasonic Detection", Nondestructive Inspection of Aging Aircraft, SPIE Vol.2001, (1993).
19. **K. F. Nilsson, and J. W. Hutchinson**, " Interaction Between A Major Crack and Small Crack Damage in Aircraft Sheet Material", International Journal of Solids and Structures, Vol.31 No.17, pp. 2331-2346, (September 1994).
20. **C. P. Fung and J. Smart**, "Experimental and Numerical Analysis of Riveted Single Lap Joints", Proceedings of the Institution of Mechanical Engineers, Journal of Aerospace Engineering, Vol.208, No.2, pp. 79-80, (1994).
21. **Montrose, Cameron**, Non-Contact Surface Flaw Inspection, M.A.Sc. Thesis, University of Windsor, (1988).

22. **P. A. Aylesworth**, Dynamic D Sight for Measuring Surface Vibration, M.A.Sc. Thesis, University of Windsor, (1993).
23. **J. M. Carlyle**, "Experiences in Testing A Fleet of Aging Aircraft Using An Acoustic Nondestructive Testing Technique", Nondestructive Inspection of Aging Aircraft, SPIE Vol.2001, (1993).
24. **Alcott, J.**, An Investigation of Non-destructive Inspection Equipment: Detecting Hidden Corrosion on USAF Aircraft, Materials Evaluation, pp.64-73, (January 1994).

VITA AUCTORIS

NAME	Qin Geng
PLACE OF BIRTH	Beijing, China
YEAR OF BIRTH	1967
EDUCATION	Dept. of Mechanical Engineering Beijing Polytechnic University, Beijing, China 1986-1991 B.A.Sc. Dept. of Mechanical and Materials Engineering University of Windsor, Windsor, Ontario 1994-1996 M.A.Sc.